공학석사학위논문

그래핀과 Bi_2Te_3기판 계면에서의 열물성 측정

Measurement of Thermal Properties at the Interface of Graphene and Bi_2Te_3 Substrate

2018 년 8 월

서울대학교 대학원

기계항공공학부

편 경 록

Measurement of Thermal Properties at the Interface of Graphene and Bi_2Te_3 Substrate

Kyung Rok Pyun
School of Mechanical and Aerospace Engineering
Seoul National University

Abstract

Graphene, a two-dimensional hexagonal honey comb lattice, has been attracted tremendous attentions due its extremely high thermal and electrical, mechanical properties. Owing to these superior properties, there have been many attempts to exploit graphene to practical applications since it was discovered in 2004. Among many research area, thermoelectric field is known as one of the promising research field that graphene can be applied.

On the other hand, bismuth telluride (Bi_2Te_3) is one of the representative thermoelectric materials due to the high thermoelectric performance at the room temperature. For this reason, Bi_2Te_3 has been already used in various research area and commercial devices, such as thermoelectric generator, peltier cooler.

Recently, a Graphene-Bi_2Te_3 composite, synthesized in the thermoelectric field, has been experimentally proved to exhibit an enhanced thermoelectric

performance. This is due to the reduced overall thermal conductivity at the composites. The additional phonon-scattering at the interface of graphene and Bi_2Te_3 is thought to be a possible factor for this reduced thermal conductivity. However, the concrete mechanism why overall thermal conducivity of composites was ruduced is not fully understaned.

Generally, thermal properties at the interface of composite are believed to play an important role in the thermal transport in composite materials. Therefore, it is important to know thermal properties at the interface to understand thermal transport in the composite. In this paper, the thermal properties, particularly thermal contact conductance (G_c) and graphene thermal conductivity (k_g), considered as important factors to the reduced thermal conductivity in the composite, were measured.

In many study pertaining to the supported graphene, they empolyed an optothermal Raman technique to measure thermal properties of supported graphene. One of the major difficulties of the optothermal Raman technique for supported graphene is how to obtain the absorptivity of graphene and the substrate. For many studies, the absorptivity of suspended graphene was equally used as the absorptivity of supported graphene. However, absorption value can be changed depending on the type of substrate like semi-conductor or conductor. This is because the electric field inside the material can be changed and influence on the

absoprtion values of sample. Therefore, the absorption values should be estimated exactly for the supported graphene. We estimated absorptivities using the Fresnel's equation from the refractive index of each matrial. This obtained absoprtion values were used in our experiment.

In short, meausring thermal contact conductance between graphene and Bi_2Te_3 and thermal conductivity, we expected that these result values would be applied to further reasearch in designing optimizing graphene-Bi_2Te_3 composites and optimizing its performance.

Keywords: thermal conductivity, thermal contact conductance, optothermal Raman technique, CVD graphene, bismuth telluride, finite-difference method, graphene conformity

Student Number: 2016-24783

Contents

List of Tables

List of Figures

Nomenclature

G	cross-plane direction heat transfer coefficient (W/m^2 K)
h	convection heat transfer coefficient (W/m^2 K)
I	height of Raman peaks (arbitrary unit)
k	thermal conductivity (W/m K)
l	length (m)
NA	numerical aperture of the objective lens
P	laser power (W)
Q	laser power (W)
R	reflection of light
T	transmission of light
$\mathbf{q}''$	heat flux (W/m^2)
r	radial distance from the origin of cylindrical coordinate system (m)
r_0	Gaussian beam radius (m)
t	thickness (m)
T	temperature
z	vertical coordinate in cylindrical system (m)

Greek symbols

α	optical absorbance (%)

λ	wavelength (m)
θ	angular coordinate in cylindrical system (rad)
ω	Raman peak position (cm^{-1})

Subscripts

2D	Raman 2D peak
a	Ambient
c	Contact
cal	calculation
exp	Experiment
g	graphene
in	input
G	Raman G peak
m	measured
sub	substrate

Chapter 1

Introduction

1.1 Backgrounds

Thermoelectric (TE) materials have greatly received attention due to its capacity of generating electricity from wasted heat. Among them, Bi_2Te_3, a rhombohedral crystal structure of bismuth (Bi) and tellurium (TE) (Teweldebrhan et al., 2010), is a representative TE material because of its high thermoelectric performance at the room temperature (Snyder et al., 2008). Bi_2Te_3 is already widely used in the various practical area such as cooling device (Park et al., 2017; Yim et al., 1972), energy generator (Jeong et al., 2017; Kim et al., 2017) and so on. Despite the possibility of being used in the practical area, the efficiency of thermoelectric device is not good as that of material. Thus, the efficiency of material is needed to be improved compared to the current level. Thermoelectric performance of TE material is defined as a dimensionless figure of merit, $ZT = \frac{\sigma S^2 T}{k}$, where σ is the electrical conductivity, S is the seebeck coefficient, T is the absolute temperature and k is the thermal conductivity. One of the well-known method to increase ZT value is lowering the thermal conductivity with maintaining the electrical conductivity and seebeck coefficient. Based on this

method, there have been many studies to improve the thermoelectric efficiency of Bi_2Te_3 (Beyer et al., 2002; Kim et al., 2006; Venkatasubramanian et al., 2000).

On the other hand, graphene, an allotrope of carbon in form of one-atomic thick sheet (Geim et al., 2007), is known as a promising material that can be applied to various area. Many studies pertaining to graphene revealed that graphene has intrinsically extremely high physical properties such as electrical (Seol et al., 2010), thermal properties (Balandin et al., 2008) compared to other traditional materials. Due to its extremely superior properties, graphene has great potential applications. Recently, several studies have attempted to convert graphene into the TE materials (Anno et al., 2017; Wang et al., 2011; Xiao et al., 2011), since it is possible that thermoelectric efficiency can be enhanced with reducing thermal conductivity of graphene (Lee et al., 2017; Cahill et al., 2014; Nika et al., 2009).

Recently, it has been experimentally validated that the composite of graphene and Bi_2Te_3 exhibits an enhanced thermoelectric performance compared with each efficiency (Agarwal et al., 2016; Ju and Kim, 2016; Li et al., 2010; Liang et al., 2013). In this composite, electrical properties were maintained about same level or slightly reduced on account of the low energy barrier between graphene and Bi_2Te_3. This low energy barrier at the interface allows the electron to penetrate the interface with ease (Agarwal et al., 2016). While the composite exhibits the lowered thermal conductivity attributed the interfacial phonon scattering at the

interface between two materials. It is evident that additional phonon scattering induced by boundaries, impurities lowers the amount of thermal transport (Dong et al., 2013; Wang et al., 2011; Xie et al., 2009). In contrast with electrical properties, relatively little research has been carried out on the quantitative measurement pertaining to thermal transport at the graphene/Bi_2Te_3 interface.

Thermal conductivity of graphene (k_g) and Thermal contact conductance (G_c) is considered as major factors which plays an important role in the thermal transport at the interface (Yue et al., 2015). While in-plain thermal transport in 2D material is influenced by in-plain thermal conductivity of material, out of plain thermal transport is dominated by thermal contact conductance between 2D material and substrate. Therefore, it is essential to measure thermal properties at the interface to understand the heat conduction between two materials. However, since probing temperature difference directly is significantly challenging process to characterizing thermal contact conductance, various methods were invited to understand the thermal contact conductance at the interface (Chen et al., 2014; Chen et al., 2009; Chung et al., 2015; Hopkins et al., 2012; Mak et al., 2010; Tang et al., 2014).

1.2 Review of previous studies about properties of 2D materials

1.2.1 Previous method for thermal properties of 2D materials

Since graphene is a material which has one atomic thick layer, it is very difficult to measure properties of graphene. Due to its ultra-thin thickness, various methods for thin film materials were applied and various new methods were invented for the measurement of thermal properties of 2D materials such as graphene and MoS_2. 3ω method, widely used method for thin film material, was applied to the graphene (Mak et al., 2010). However, 3ω method requires electric circuit to heat the sample and the thickness of electric circuit should be smaller than the thickness of graphene for the accuracy. This set-up of circuit is almost impossible considering thickness of graphene. Also, scanning thermal microscopy was invented to measure thermal properties of graphene (Chung et al., 2015). However, experimental set-up is very difficult and high resolution is needed for the measurement. Other methods for 2D materials such as pump and probe method was can be applied (Hopkins et al., 2012). However, these methods have some disadvantages like previous method.

1.2.2 Measurement of thermal properties of 2D materials using a Raman spectroscopy

As a method for characterizing thermal properties, Raman spectroscopy based technique is considered as an efficient tool for the two-dimensional (2D) materials

(Ferrari et al., 2013). Many research groups employed Raman spectroscopy based technique to measure the thermal conductance between 2D material and the substrate. Thermal conductance of graphene/4H-SiC (Yue et al., 2011), MoS_2/h-BN and graphene/h-BN (Liu et al., 2017) is measured using joule heating and Raman probing method. Joule heating method can provide a wide range of heating power and uniform heat to the sample. However, the electrical heating is required to build electrical circuits on the sample. This fabrication of electrical circuit may cause a sample damage and unexpected additional thermal resistance. Also, an additional laser heating and Raman probing method is exploited to measure thermal conductance of graphene/SiO_2 and graphene/Si (Tang et al., 2014) and graphene/SiC (Tang et al., 2014). This additional heating method have the merit of being free from the fabrication of electric circuits and any physical touch during the experiment. Furthermore, experimental uncertainty can be reduced in this method due to the wide disparity between heating area and probing area. Despite these advantages of heating laser, the first experimental set-up would be an expensive and time-consuming process.

1.3 Overview

In Chapter 2, the procedure to prepare sample is presented. Synthesis of graphene and Bi_2Te_3 is presented, including method for graphene transfer to the substrate. Characterization of synthesized samples were implemented using

scanning electron microscopy, Raman spectroscopy, Raman mapping and optical microscopy.

In Chapter 3, an opto-thermal Raman technique with two different objectives are introduced in detail. Previous opto-thermal Raman technique is improved by considering absorptivity of supported graphene and its substrate coincidently. Furthermore, method for extracting absorptivity of supported graphene and its substrate is also introduced in this chapter.

In Chapter 4, results of opto-thermal Raman technique is presented. The correlations essential to the opto-thermal Raman technique is measured in this chapter. Moreover, repeatability and accuracy for improved method is verified in this chapter.

Chapter 2

Sample Preparation and Characterization

2.1 Synthesis of graphene

We synthesized single-layer graphene by using chemical vapor deposition (CVD) system. Among various method for synthesizing graphene, CVD system is most widely used method, having a great advantage of synthesizing large-area graphene.

CVD synthesis of graphene requires a precursor gas that contains carbon and a heat source that provides energy for thermal decomposition of hydrocarbon precursor gas. Since thermal decomposition temperatures of carbon sources are very high, imposing a severe limitation on the system, a transition metal catalyst is preferred as the growth bed. Schematic of CVD is described in Figure 3.1. Gas phase reactant is transported to the reaction zone, followed by thermal decomposition, diffusion, and reaction at the surface of the catalyst, subsequently desorbed and pumped away.

2.1.1 CVD system

Figure 2.1 shows the schematics of CVD system employed in our graphene synthesis. CVD system is composed of a quartz tube (inner diameter of 100 mm)

and a furnace surrounding the quartz tube. The furnace heats inside of the quartz tube through radiative heat transfer. All reactions to grow graphene occur in the heated quartz tube. H_2 and CH_4 gases were used as precursor gases. H_2 and CH_4 gases are supplied from each gas cylinder, controlled by a pressure regulator and a mass flow rate controller (CG2000, ATOVAC). A capacitance manometer (MKS Instruments) and a K-type thermocouple (Omega) monitors and displays pressure and temperature of the inside of quartz tube. A rotary pump (750 W, W2V40, Woosung Automa) is linked at the end of the chamber, making low pressure inside of the chamber. For safety purpose, a gas detector/alarm system keeps any flammable H_2 or CH_4 gases from leaking.

2.1.2 CVD synthesis of graphene

When synthesizing graphene via CVD system, parameters such as temperature, growth time, volumetric flow rates of precursor gases H_2 and CH_4 influence the growth of graphene. At our previous works, we already set a condition for the single-layer graphene and this condition was used in this study (Kim et al., 2017). The procedure to synthesize the single-layer graphene is as follows: First step is for pre-cleaning the substrate. The commercially available 25-㎛-thick copper foil (Alfa Aesar, 99.999% purity) was used as the catalytic substrate. In order to pre-clean the copper foil, the copper foil was inserted into Nickel Etchant (Transene Inc.) for 30 seconds. Then, the copper foil was submerged by deionized water (DIW) 3 times and for 120 seconds each time to remove remaining Nickel Etchant.

Second step is for the growth of graphene on the substrate. The pre-cleaned copper foil was loaded into the CVD chamber, then the chamber was instantly evacuated to the extremely low pressure of 10^{-4} Torr. As 5 sccm of H_2 gas was flowing, the temperature of the chamber is raised to 1000 ℃ in 60 minutes. When the temperature of the chamber reached 1000 ℃, the copper foil was annealed for 40 minutes at the same temperature. After annealing, 30 sccm of CH_4 was released with 5 sccm of H_2 for 15 minutes at the pressure of 3.4×10^{-1} Torr. Then, the flow rate of CH_4 was changed to 60 sccm at the pressure of 5.8×10^{-1} Torr. Lastly, the grown graphene and the chamber were cooled to the room temperature for 100 minutes with 1.5 sccm of H_2. Finally, Ar gas was flowed for 5 min to neutralize the chamber and the sample.

2.2 Synthesis of bismuth telluride

Bismuth telluride (Bi_2Te_3) also synthesized by using Bridgman method for this work. However, Bi_2Te_3 used in this work synthesized at Ehwa university team with which we collaborate. Therefore, the method for synthesizing Bi_2Te_3 is briefly introduced in this section.

2.2.1 Bridgman synthesis of Bi_2Te_3

Single crystals of Bi_2Te_3 were grown in a Bridgman furnace. Appropriate amounts of element Bi (99.999%, Alfa Aesar) and Te (99.999%, Alfa Aesar)

loaded into evacuated silica tube (14 mm diameter, 1 mm wall thickness) according to the stoichiometry of Bi_2Te_3, and then sealed under vacuum. The sealed silica tube was heated at 1100 ºC for 12 h in order to homogenize the melts, cooled to 800 ºC over 12 h, and then dwelled at the same temperature for 12 h. Then, it was gently pulled down to room temperature by the rate of 2.3 mm/h. The resulting dense ingots were about 20 mm long, approximately 14 mm in diameter, well cleavable, and their cleavage plane was always perpendicular to the pulling direction. The cast ingot samples were powdered by ball milling in an Ar-filled glove box and the ground powder was passed through a 53 μm-mesh sieve. The powder was consolidated using a spark plasma sintering (SPS) technique (SPS-211Lx, Fuji Electronic Industrial Co., LTD, Japan) to obtain dense bulks. Typically, 12–13 g of the powdered samples were loaded in a graphite die with an inside diameter of 14 mm and heated to 425 ℃ for 5 min at a heating rate of 100 ℃/min and held there for 5 min under an axial pressure of 50 MPa under a vacuum of 1.4×10^{-2} Torr. After sintering, disk-shaped pellets with a diameter of ~ 14 mm and thickness of ~ 10 mm were obtained. The resulting samples were mechanically polished with successive finer grades of sand papers from 100 to 1200 in ethanol, followed by a velvet cloth using alumina paste to obtain a mirror-like finish.

2.3 Graphene transfer to the bismuth telluride substrate

The CVD grown single-layer graphene on the copper foil was transferred to the Bridgman synthesized Bi_2Te_3 substrate using polymethyl-methacrylate (PMMA) (Suk et al., 2011). The CVD graphene on the cu foil was spin-coated by PMMA at 4000 rpm for 45 seconds. Then, it was heated on a hot plate at 160 ℃ for 90 seconds. We used ammonium peroxydisurfate as a copper etchant (500ml of DI water + 13g of ammonium peroxydisurfate). The copper foil was removed by the copper etchant for 2-3 hours. After the copper foil is perfectly removed, PMMA coated graphene was rinsed with DI water 3 times for 30 minutes each time. Then, PMMA coated graphene was moved to the Bi_2Te_3 substrate and heated at 120 ℃ for 20 minutes. PMMA was removed in acetone for 1 hour 30 minutes. Lastly, graphene was submerged in isopropyl alcohol for Then, graphene on substrate was dried at the ambient condition and the vacuum 30 minutes each time.

2.4 Vacuum annealing

After graphene transfer, the sample was vacuum annealed in vacuum chamber. For measuring thermal contact conductance, a conformity between graphene and substrate is very crucial. After transfer process, molecules such as H_2O, air

remains between graphene and substrate, these intercalated molecules can influence on the contact at the interface of graphene and substrate. Therefore, the contact quality is very important factor to decide thermal properties at the interface. Generally, it is known that annealing process makes better the conformity as schematically depicted in Figure 2.2 (Ryu et al., 2010; Kim et al., 2018). Since it was revealed that vacuum annealing shows better conformity compared to the ambient annealing, the final sample was annealed in vacuum chamber at 150 ℃ for 30 min. Through the vacuum annealing, we secured the conformity between graphene and Bi_2Te_3 graphene. Moreover, vacuum annealing makes much more analogous conditions of the composites, graphene sandwiched in the Bi_2Te_3 matrix with few molecules. Thus, the contact area could be considered as one layer of micro-scale composite at least in the laser beam radius.

2.5 Characterization

After the sample preparation, we need to confirm whether sample quality is good or not. Various methods were used to verify that single-layer graphene is made well, or that graphene is transferred to the target substrate or not. In this section, scanning electron microscopy (SEM), Raman spectroscopy, Raman mapping, optical microscopy methods were used to characterize synthesized graphene.

2.5.1 Scanning electron microscopy (SEM)

The scanning electron microscopy (SEM) image is employed to verify whether graphene is fully grown on the copper foil. This is because since graphene growth starts from seeds on the copper foil, there is a possibility that graphene does not fully cover the copper foil. Figure 2.3 shows SEM images of graphene on the copper foil. In the inset of Figure 2.3, SEM image is separated into white part and black part. The inset image is the graphene which is not fully grown in the CVD system. The white part is copper foil with no grown graphene. The black part is synthesized graphene. From the SEM image, although there are some impurities on the graphene, we can observe that graphene fully cover the copper foil.

2.5.2 Raman spectroscopy

Raman spectroscopy has various functions such as material identification, temperature measurement, doping concentration and so on. One of the major function of Raman spectroscopy is the material identification. Applying this function to graphene, we can verify whether synthesized sample is graphene or whether synthesized graphene is single-layer or not. Typically, it is well known that Raman spectrum of graphene has two types of conspicuous peaks. One is G peak whose position is about 1560 cm^{-1}. G peak is observed due to the vibration of sp2 bonding in carbon. The other is 2D peak that can be observed near 2700 cm^{-1}. It is known that double scattering of phonon arises 2D peak. Figure 2.4

indicates Raman spectroscopy of our graphene just after transferred to the Bi_2Te_3 substrate. As explained, we can observe G peak and 2D peak at the Raman spectrum. Therefore, we can confirm that the synthesized sample is graphene.

Also, it is known that the ratio of 2D peak intensity to G peak intensity (I(2D)/I(G)) of single-layer graphene is larger than 2 (Das et al., 2008; Huang et al., 2010; Yang et al., 2009). In this Raman spectroscopy, intensity ratio I(2D)/I(G) which is higher than 2 is observed. Therefore, the synthesized graphene can be considered as a single-layer graphene.

2.5.3 Raman mapping

The Raman mapping is a process that obtains Raman spectroscopy in a large area. After obtaining Raman spectroscopy, results are displayed in a picture with a shaded bar. Figure 2.5 represents the Raman mapping of our sample. After graphene transfer to the Bi_2Te_3 substrate, we performed the Raman mapping process at an area of 30 μm × 30 μm with resolution of 2 μm × 2 μm. The laser irradiated with 0.02mW power during 90 seconds per each points. Total number of Raman spectroscopy that constitutes the Raman mapping is 625 points. From the Raman mapping, we can conclude that the synthesized graphene was successfully transferred on the Bi_2Te_3 substrate. Moreover, we can verify that synthesized graphene has a large-area to perform the experiment.

Also, we can check whether the synthesized graphene is single-layer or not from the Raman mapping. As mentioned in section 2.5.2, the intensity ratio of

I(2D)/I(G) can be an indicator that certify the number of graphene layer. The average intensity ratio of I(2D)/I(G) was 2.286, which demonstrates graphene is single-layer. Even though it does not have extremely uniform the intensity ratio of I(2D)/I(G), it is enough high value to decide that the monolayer graphene is successfully synthesized.

2.5.4 Optical microscopy

Additionally, we can also characterize our sample with optical microscopy. It does not give us any concrete data to analyze. However, the optical microscopy is very crucial to decide the status of sample such as surface roughness, defect and so on. Figure 2.6 shows the optical image of our sample just after graphene transfer. Some cracks are observed at the surface of Bi_2Te_3 substrate, it does not much matter for the opto-thermal Raman technique. Since the opto-thermal Raman technique is based on the point measurement, if we take clear circular surface having a radius of decades of micrometers, decent quality of Raman spectroscopy can be obtained. From the optical image, it is observed that our sample have enough clear surface to perform the experiment. Moreover, we can also find graphene-Bi_2Te_3 boundary at the optical images, which shows successful graphene transfer.

2.6 Conclusion

CVD system and Bridgman method have been employed to synthesize single-layer graphene and Bi_2Te_3 substrate, respectively. Figure 2.7 describes all procedure to prepare final sample. Synthesized single crystalline Bi_2Te_3 ingot was ball-milled to obtain micro-nano scale Bi_2Te_3 powder. Then, Bi_2Te_3 powder was sintered into the bulk substrate. These procedure is implemented to make similar surface condition with the composite of graphene-Bi2Te3, since the composite with enhanced performance has micro scale of Bi_2Te_3. Furthermore, the sample was vacuum annealed after graphene transfer to make better conformity with substrate. Inset of Figure 2.7 shows optical image of final sample for the experiment.

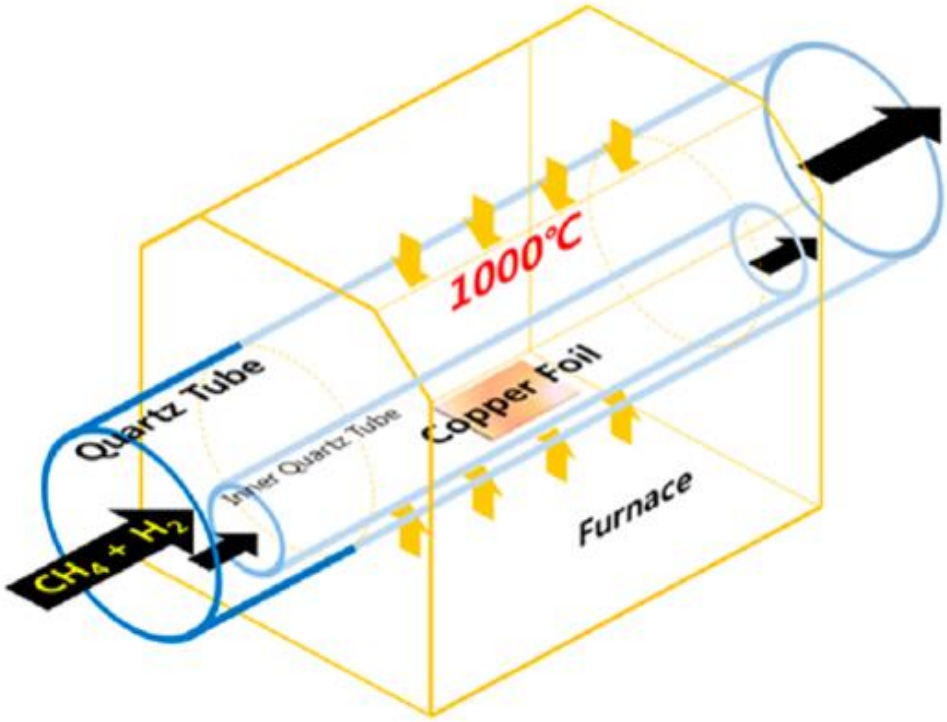

Figure 2.1 Schematics of CVD system for graphene synthesis

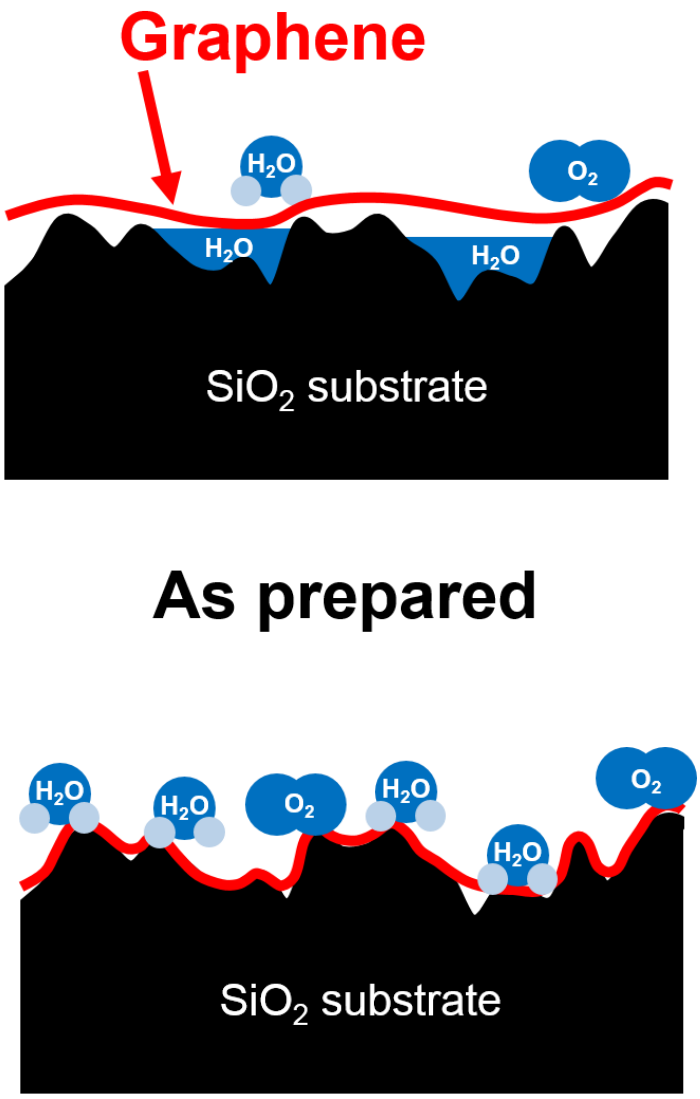

Figure 2.2 Schematic comparison of graphene conformity before annealing (above), and after annealing (below).

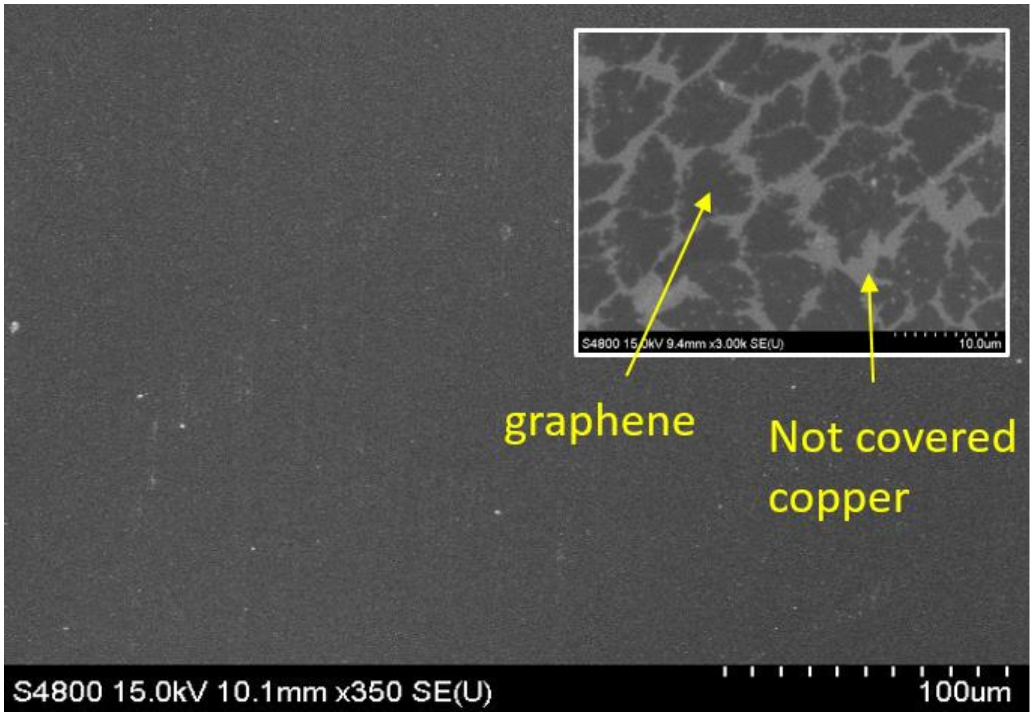

Figure 2.3 SEM image of fully grown graphene (Inset : SEM image of not fully grown graphene)

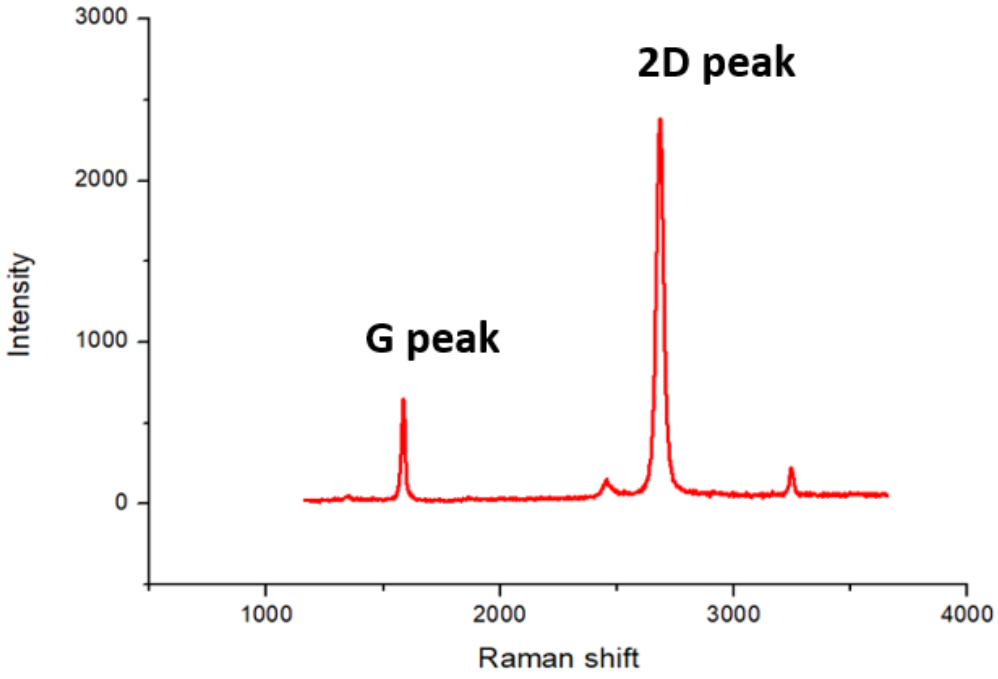

Figure 2.4 Raman spectroscopy of graphene on the Bi_2Te_3 substrate.

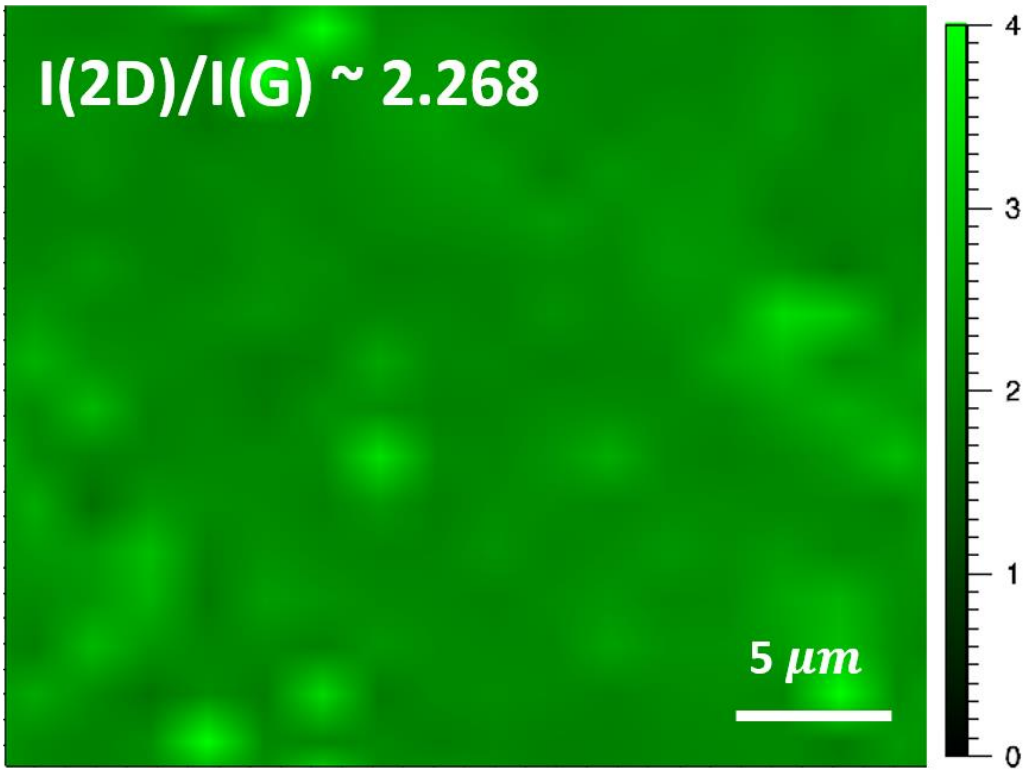

Figure 2.5 Raman mapping of graphene on the Bi_2Te_3 substrate. (I(2D)/I(G))

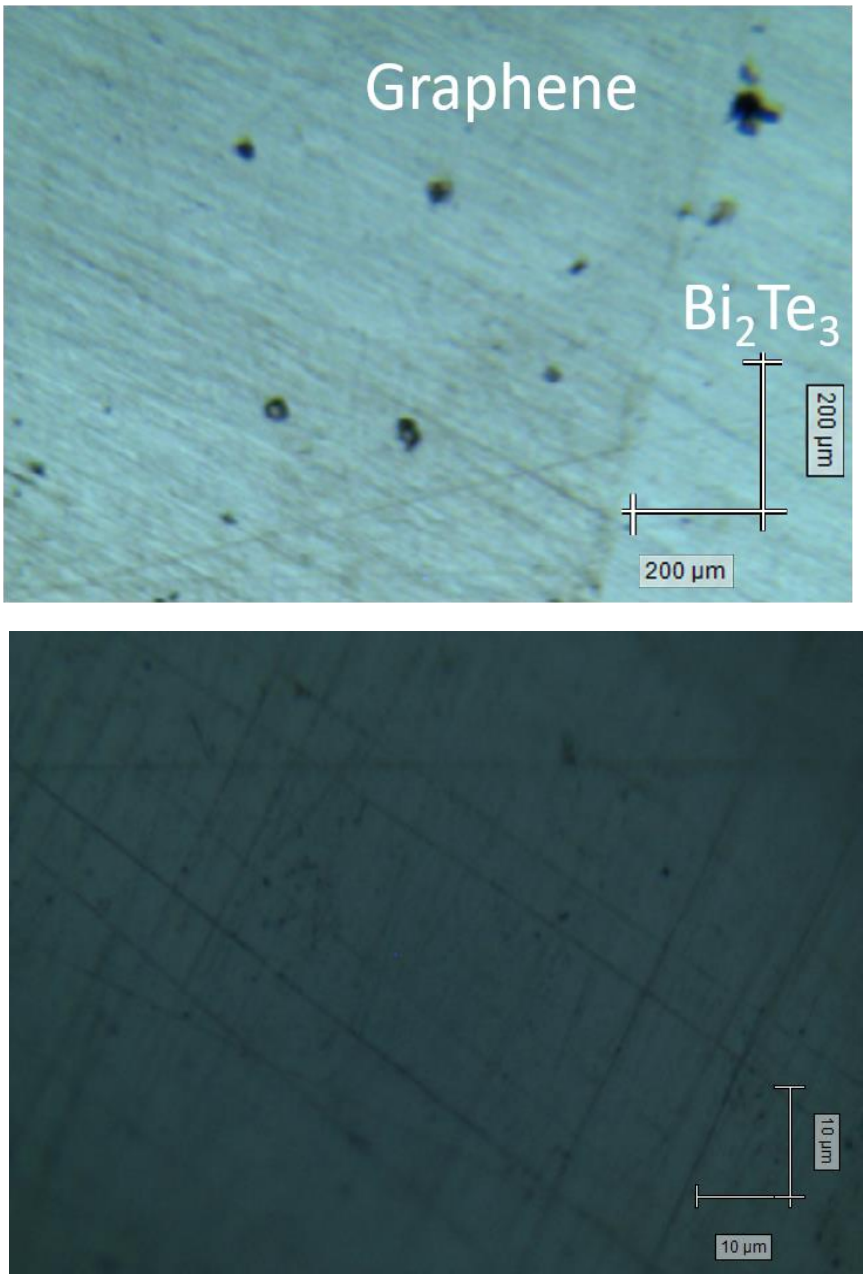

Figure 2.6 Optical microscopy of graphene on Bi_2Te_3 substrate.
5× (above), 100× (below)

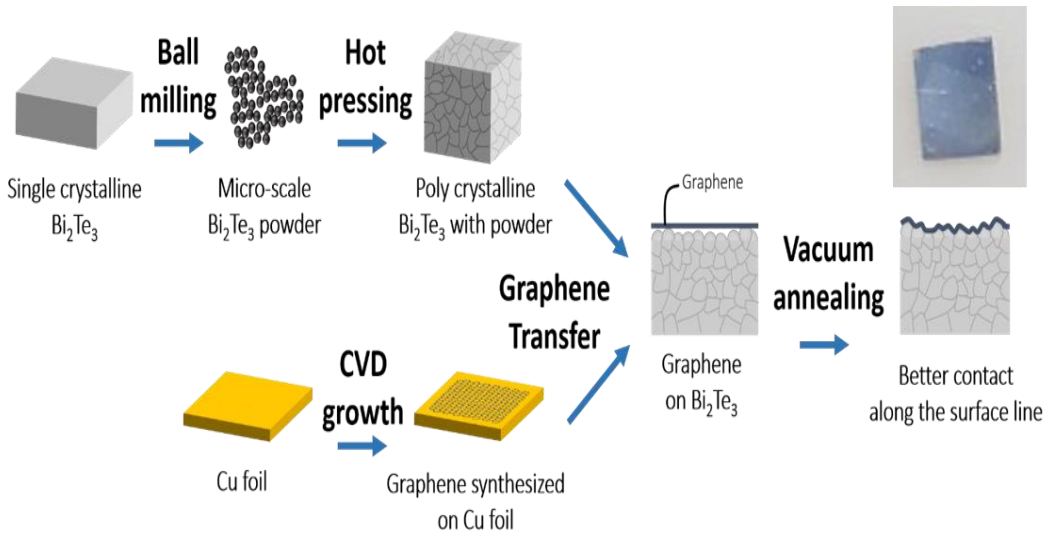

Figure 2.7 Procedure for sample preparation. (Inset : Actual image for final sample)

Chapter 3

Experimental Method

3.1 Introduction

Measurement of thermal properties of graphene has been a great challenge compared to those of bulk material due to its ultra-thin thickness. For this reason, various methods were invented to measure thermal properties of graphene such as thermal conductivity, thermal contact conductance with the substrate and so on. The representative methods for measurement thermal property of graphene are 3 omega method (Mak et al., 2010), scanning thermal microscopy (Chung et al., 2015), pump probe method (Hopkins et al., 2012). However, an opto-thermal Raman technique has been considered as an efficient tool for measuring thermal properties of graphene, since it was invented (Balandin et al., 2008, Ferrari et al., 2013). This is because it does not require any sample preparation like electrical circuits and any contact with experimental equipment.

Although it is the opto-thermal technique is an excellent method for graphene, it has some challenges for the supported graphene. Unlike the suspended graphene, the supported graphene entails thermal transport to the substrate. Therefore, the 2D heat transfer modeling used for suspended graphene is not applied for the supported graphene.

Moreover, one of the difficulties of the opto-thermal Raman technique for supported materials is that there is no direct method to obtain absorption value of graphene and substrate (Judek et al., 2015). Actually, our method is based on the opto-thermal Raman technique with different beam spot radius to spontaneously extract thermal conductance and thermal conductivity of 2D material with its substrate, borrowing previously reported method (Judek et al., 2015; Taube et al., 2015). However, previous research made a mistake when they apply absorptivity of supported 2D material to their governing equation. Since light absorbance is the only heat source at the sample, it is important to know absorptivity of supported 2D material. In the section 3.4, we improved the opto-thermal Raman technique by extracting absorptivity of supported 2D materials

To solve these difficulties, we established 3D heat transfer modeling in this chapter. Additionally, noticeable thing in this chapter is that how to obtain absorption values of supported graphene and it substrate. From the refractive indices of sample and Fresnel's equation, absorption values of sample were estimated.

3.2 Opto-thermal Raman technique with two different objectives

Basically, the opto-thermal Raman techqniue consists of two experimental procedures. Measurement of thermal properties using the opto-thermal Raman technique adopts both temperature measurement experiment and numerical

calculation to solve governing equation for given system.

3.2.1 Raman thermometry

Our experimental schematics of Raman micro-spectroscopy is shown at Figure 3.1. Raman micro-spectroscopy system with 514 nm laser (Renishaw inVia-reflex model with 100× 0.75 NA and 20× 0.4 NA objectives) was employed in our experiment. A single-layer graphene laid on the Bi_2Te_3 (500 μm) substrate was also prepared. In fact, this method is based on previous works using two different beam sizes. When the heating laser is irradiated to the graphene, the heat induced by laser is dissipated to the in-plain direction and cross-plain direction. Graphene temperature would be determined depending on magnification of objective and properties of sample due to heat absorption and dissipation in the sample. In this method, graphene temperature can be measured by examining Raman spectrum of graphene. As represented in Figure 2.4, Raman spectrum of graphene. Graphene has two major peak, G peak and 2D peak. The position of these peaks has linear dependence to the temperature. Using the relation between position of peak and temperature, and incident laser power, we can measure temperature rise due to the irradiated laser. Then, we can know the temperature of graphene (T_{m_exp}). This temperature would be used in the calculation to extract thermal properties of sample.

3.2.2 Numerical calculation

On the other hand, a numerical examination is essential to extract the thermal properties of sample in our method. By considering the heat transfer at the sample, two governing equations can be established for graphene and Bi_2Te_3 substrate from the energy balance method (Cai et al., 2010). Considering all terms about incoming and outgoing heat transfer described in the Figure 3.2, governing equations for graphene and Bi_2Te_3 were established as follows. Note that we assumed that heating laser follows the Gaussian distribution that can be expressed by $\exp\left(-\frac{2r^2}{r_0^2}\right)$. Equation (3.1) is for the graphene and Equation (3.2) is for the Bi_2Te_3 substrate.

$$t_g \frac{1}{r}\frac{\partial}{\partial r}\left(k_g r \frac{\partial T_g}{\partial r}\right) - G_c\left(T_g - T_{Bi_2Te_3}\right) - h\left(T_g - T_a\right) + \alpha_g q_0'' \exp\left(-\frac{2r^2}{r_0^2}\right) = 0 \tag{3.1}$$

$$\frac{1}{r}\frac{\partial}{\partial r}\left(k_{Bi_2Te_3(\parallel)} r \frac{\partial T_{Bi_2Te_3}}{\partial r}\right) + \frac{\partial}{\partial z}\left(k_{Bi_2Te_3(\perp)} \frac{\partial T_{Bi_2Te_3}}{\partial z}\right) + \alpha_{Bi_2Te_3} q_0'' \exp\left(-\frac{2r^2}{r_0^2}\right) = 0 \tag{3.2}$$

Notable thing is that these equations were based on the diffusive thermal transport which adopts Fourier's law. It is known that a supported graphene has a few hundreds of nanometer phonon mean free path. Therefore, several times of phonon scattering can occur in the diameter of laser beam spot. These several times of scattering make it possible to assume that heat transfer phenomenon is the diffusive heat transfer. By solving these two governing equations using

MATLAB codes represented in Appendix A, we can calculate the temperature of graphene (T_g) and Bi_2Te_3 substrate (T_{sub}).

As expressed in equation (3.1) and (3.2), temperature of graphene and Bi_2Te_3 substrate are function of a set of given parameters.

$$T_g \ \& \ T_{sub} = f(G_c, k_g, t_g, k_{Bi_2Te_3}, h, r_0, Q_{in}, \alpha_g, \alpha_{Bi_2Te_3}) \tag{3.3}$$

Parameters used in equations except for G_c and k_g can be obtained from measurements or calculations. t_g is the thickness of graphene which is 0.335 nm. We measured thermal conductivity of Bi_2Te_3 substrate ($k_{Bi_2Te_3}$) for the both parallel($\parallel$) and perpendicular($\perp$) direction using LFA (Laser Flash Analysis) method. The measured $k_{Bi_2Te_{3(\parallel)}}$ and $k_{Bi_2Te_{3(\perp)}}$ at the room temperature were 1.582 W/m·K and 1.057 W/m·K, respectively. *h* is the convective heat transfer coefficient, 2.9×10^4 W/m^2K (Chen et al., 2010). r_0 is the radius of laser beam spot estimated to be $r_0=\lambda/(\pi \cdot NA)$. The estimated laser beam radius were 0.409 μm and 0.218 μm for 100× objective and 20× objective, respectively. Q_{in} is the incident laser power measured by a powermeter, 0.1 mW and 0.25 mW for 100× objective and 20× objective, respectively. Lastly, α_g and $\alpha_{Bi_2Te_3}$ are coefficients related to the laser absorption. As mentioned before, the estimation of absorption for the supported 2D material is one of the difficulties for the Raman thermometry. In this paper, absorption values were calculated by using Fresnel's equations and

measured complex refractive index values of graphene and Bi_2Te_3. An ellipsometry was exploited to estimate the refractive index of Bi_2Te_3 substrate. The obtained absorption coefficients for α_g and $\alpha_{Bi_2Te_3}$ are 0.84% and 44.08%, respectively. The details of extracting absorption values of supported graphene and its substrate will be discussed later. By solving equations with given parameters, the temperature profiles for graphene and Bi_2Te_3 substrate can be obtained simultaneously. Since we assumed the distribution of incident laser to be the Gaussian distribution, the temperature distribution caused by the laser incidence is also has Gaussian distribution. From the calculated graphene temperature with Gaussian distribution, the graphene temperature can be estimated in form of below equation.

$$T_{m\_cal} = \frac{\int_0^R T_g(r)\exp\left(-\frac{2r^2}{r_0^2}\right)rdr}{\int_0^R \exp\left(-\frac{2r^2}{r_0^2}\right)rdr} \tag{3.4}$$

The two partial differential equation provide multiple solution sets of G_c and k_g that satisfy the condition of T_{m_cal} = T_{m_exp} for each objectives. Note that T_{m_exp} is the temperature obtained from Raman thermometry. Since two different objectives were employed in this experiment, the governing equations can be applied to each lens. Therefore, two different multiple solution sets corresponding to each lens can be extracted from governing equations. Different two multiple

solution sets result from different beam radius of each lens. Having different diameter of beam spot, each lens gives different size of heating area with different power density. As expressed at Figure 3.3, different power density with different beam radius results in different shapes of the Gaussian temperature profile, which of 20× objective is wider and lower compared to that of 100× objective. This difference makes each multiple solution sets have entirely different values between two objectives. As shown at Figure 3.4, the multiple solution sets of G_c and k_g can be expressed as a solution curve in k_g vs G_c graph. However, two solution curves with different slopes give only single solution pair of G_c and k_g, which coincide with the intersection point as depicted in Figure 3.4. This single solution set of G_c and k_g can be considered as the thermal property of our sample, since property does not change significantly unless the temperature of the sample is not changed much.

3.3 Absorption value of supported graphene and Bi_2Te_3 substrate

The optical absorption on graphene and that in Bi_2Te_3 are the only heat sources of the current system Figure 3.5 (above), so the amount of them should be determined as the input of the heat transfer calculations. It is commonly known that graphene absorbs ~3% of incident light, but this is only the case when it is suspended or laid on transparent substrates. In current configuration, not only the

graphene, but also the opaque Bi_2Te_3 substrate absorbs finite amount of light, influencing the light absorption on graphene again.

Unfortunately, there is no direct measurement method that can separately detect the light absorption on graphene and/or that inside the substrate. Instead, the theoretical analysis for the three-layer reflection (*R*) and transmission (*T*) in Figure 3.5 (below) is used to calculate the absorption on the two layers. Here, the transmission from the air/graphene/Bi_2Te_3 interface (*T*) is entirely absorbed by Bi_2Te_3 because no light goes through the bottom of the Bi_2Te_3 substrate, so $T=\alpha_{Bi2Te3}$ and 1-*R*-*T* is the absorption on graphene, α_g.

R and *T*, The necessary and sufficient conditions for getting A_{Bi2Te3} and A_G, are given by the calculations based on Fresnel's coefficients, where the complex refractive indices of graphene and Bi_2Te_3 are input values and the multilayered configuration is taken into account by transfer matrix method (or infinite geometric series of multiple reflection and transmission in [3.5]):

$$R = \left| \frac{M_{21}}{M_{11}} \right|^2 \tag{3.5}$$

$$T = \frac{\mathrm{Re}\{n_3\}}{\mathrm{Re}\{n_1\}} \left| \frac{1}{M_{11}} \right|^2 \tag{3.6}$$

$$M = I_{12} L_2 I_{23} L_3 \tag{3.7}$$

$$I_{mn} = \frac{1}{t_{mn}} \begin{bmatrix} 1 & r_{mn} \\ r_{mn} & 1 \end{bmatrix} \tag{3.8}$$

$$L_m = \begin{bmatrix} \exp(-ik_{zm} d_m) & 0 \\ 0 & \exp(-ik_{zm} d_m) \end{bmatrix} \tag{3.9}$$

where r_{mn}, t_{mn}, k_{zm}, and d_m are reflection and transmission coefficients from mth to nth layer, z-component (perpendicular to the interface) of the wave vector, and the thickness of mth layer. The refractive index value of graphene is reported in the previous work as 2.65+1.27i (Cheon et al., 2014), and that of Bi_2Te_3 is measured by ellipsometry to give 1.456+2.673i. Substitution of these into the equations (3.5) to (3.9) gives R=0.5505 and T=0.4411, so $\alpha_{Bi2Te3}=T$=0.4411 (44.11%) and α_g=1-R-T=0.0084 (0.84%) are obtained.

3.4 Conclusion

In this chapter, an opto-thermal Raman technique with different two objectives is introduced in detail. Especially, numerical examination to extract thermal properties was improved in this section. First, 3D heat transfer modeling was established due to the thick substrate. Second, absorptivity of graphene and Bi_2Te_3 substrate was obtained using complex refractive index and Fresnel's equation.

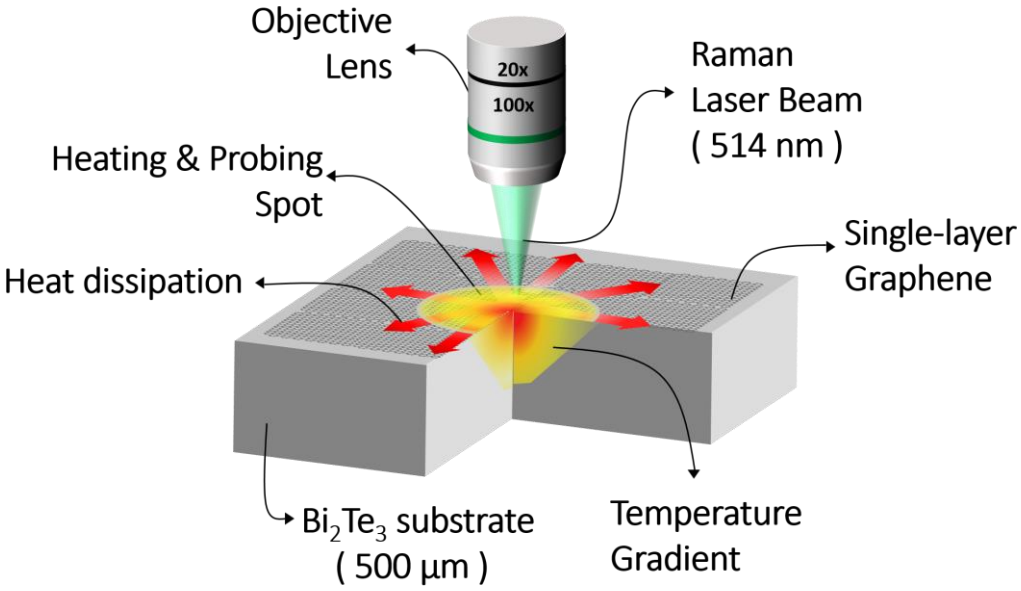

Figure 3.1 Schematics of an opto-thermal Raman technique

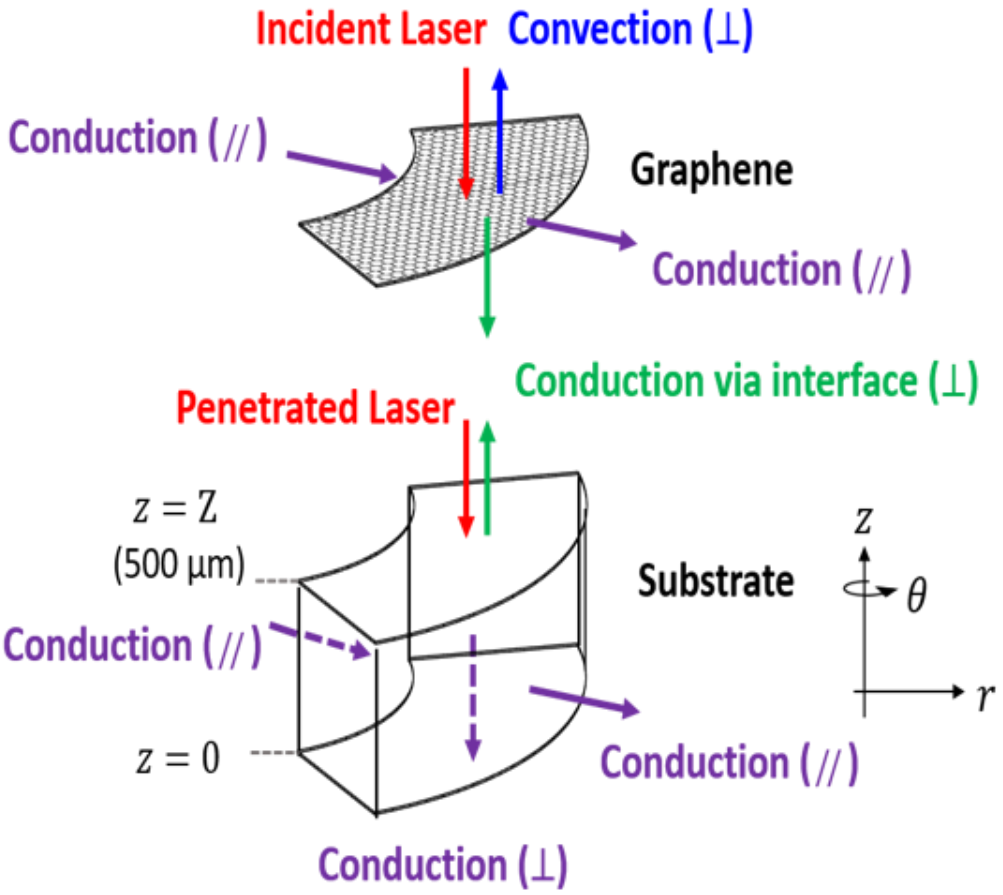

Figure 3.2 3D heat transfer modeling for numerical calculation

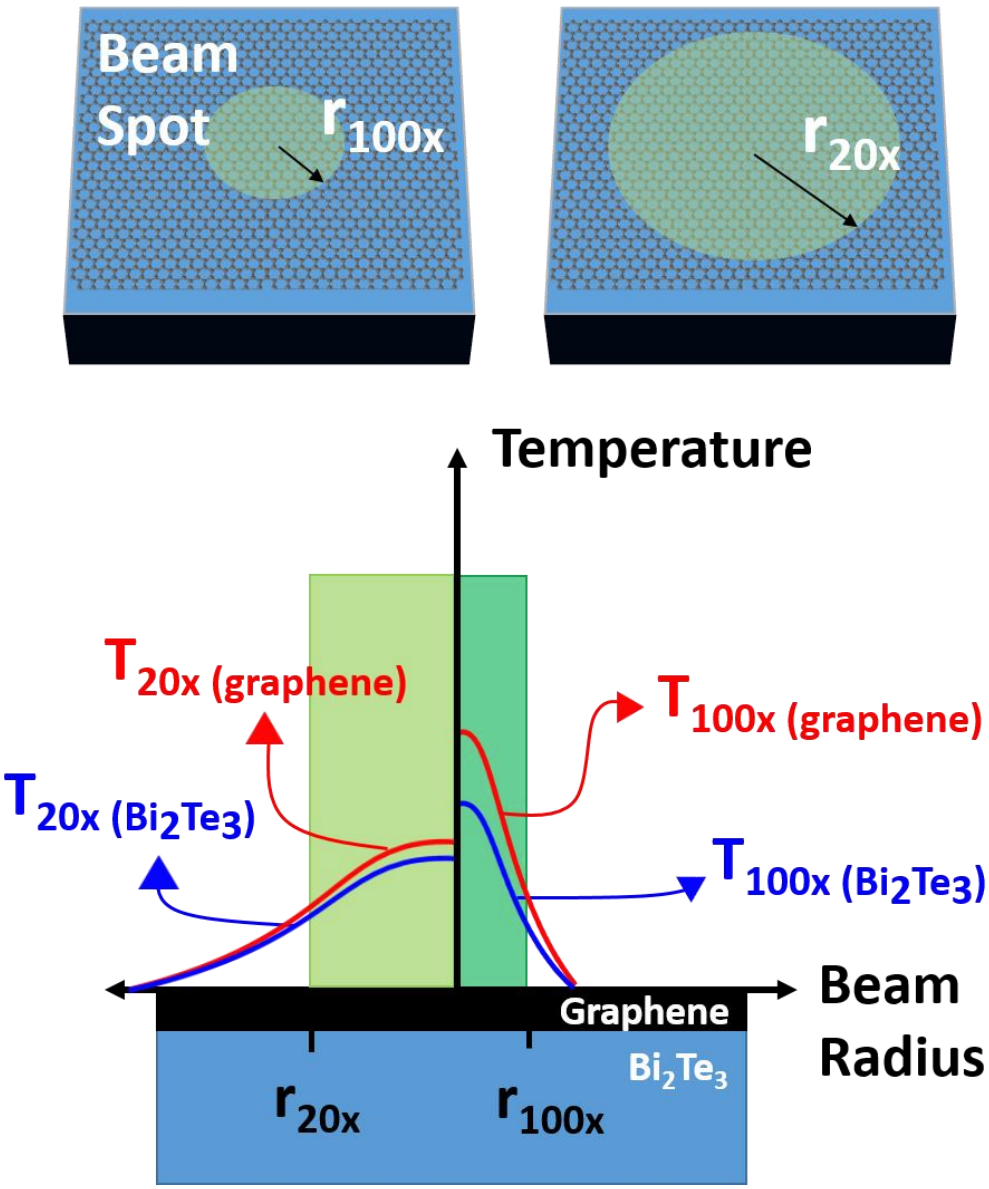

Figure 3.3 Different temperature distribution due to the difference of beam diameter of objectives

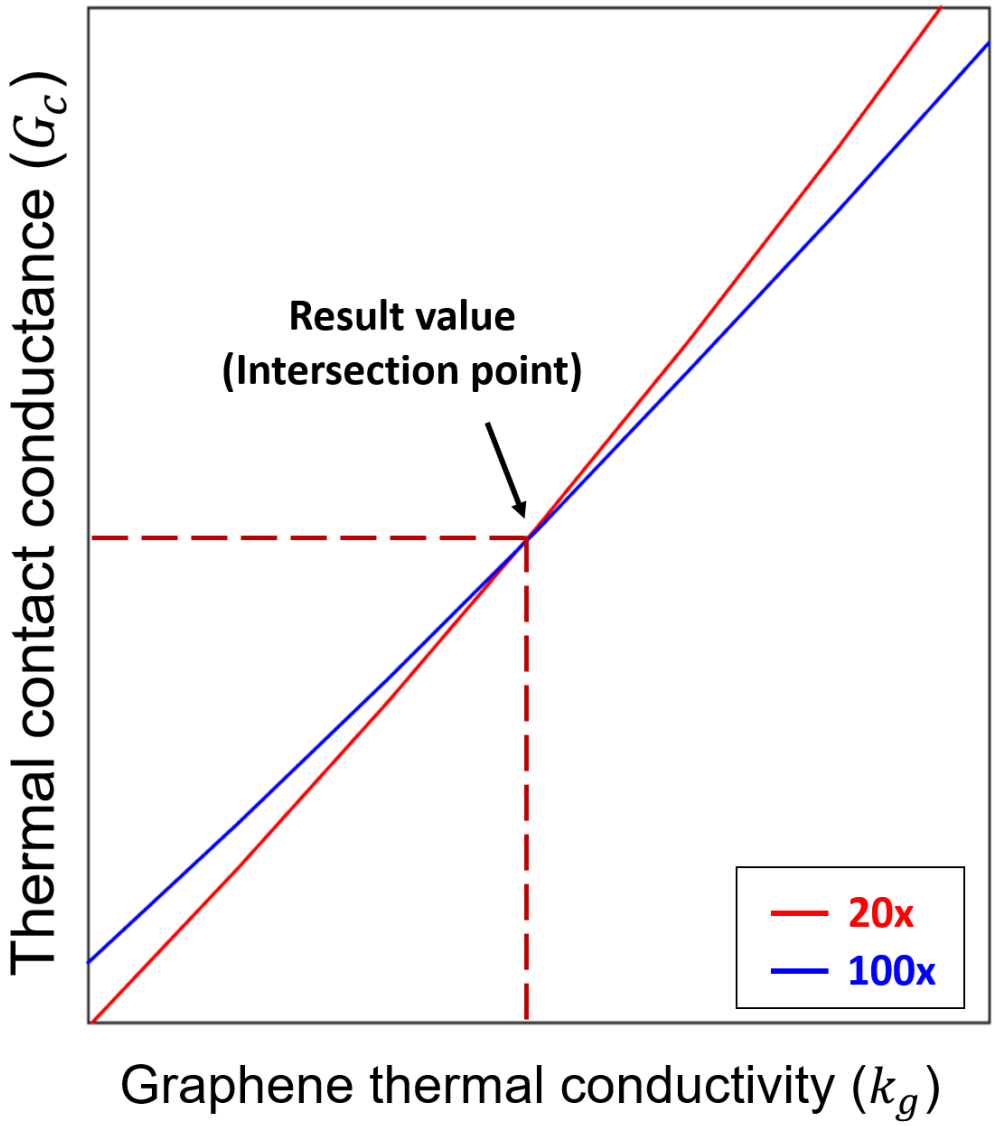

Figure 3.4 Two solution curves for governing equations from each objective and its intersection point

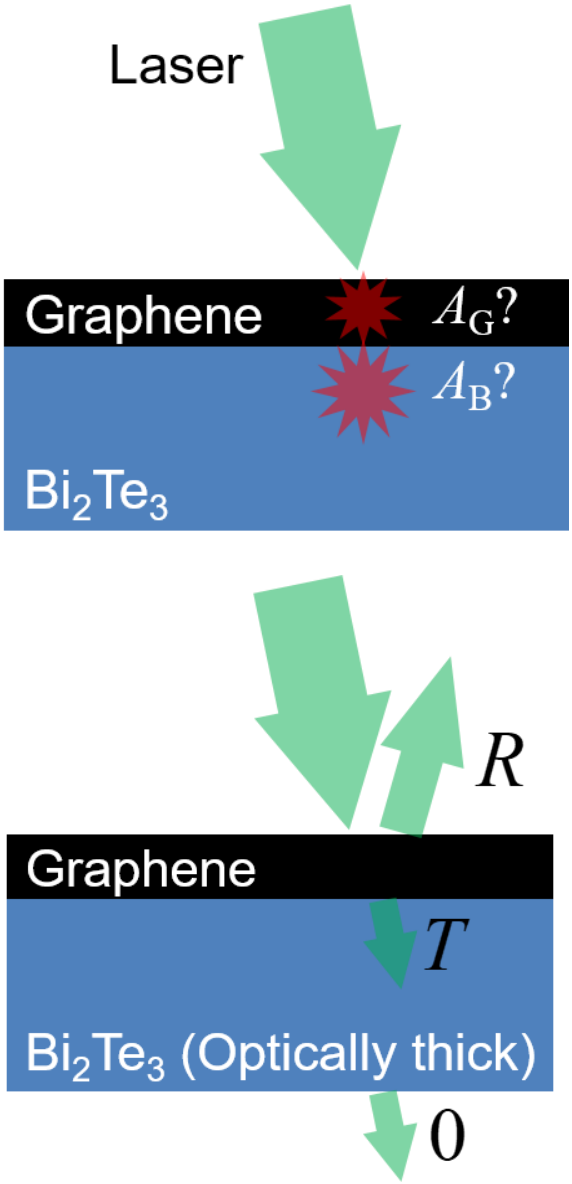

Figure 3.5 Schematics for light absorption of graphene and its substrate (above), Schematic description for light transmission and reflection (below).

Chapter 4

Results and Discussion

4.1 Introduction

In this chapter, the detailed sequent experimental results pertaining to the opto-thermal Raman technique (Chapter 3) are represented. The sample prepared in previous section (Chapter 2) was used for the measurement. The detailed procedures of the opto-thermal Raman experiment already introduced at the previous chapter.

The opto-thermal Raman technique requires two-steps of experiment. First step is a calibration process (section 4.3). Second step is a heating process (section 4.4). Through these two steps, we can measure the temperature of supported graphene. This is so-called Raman thermometry. Through these procedures, Thermal conductivity of graphene (k_g) and thermal contact conductance between graphene and Bi_2Te_3 substrate (G_c) were extracted in this chapter.

4.2 Position of Raman 2D peak depending on temperature

As mentioned before, the opto-thermal Raman technique entails two steps of experiment. This section deals with first step related to the Raman calibration. The

calibration process should be performed whenever measuring point and sample were changed. This is because each sample has different thermal expansion values related to temperature coefficient ($d\omega/dT$), which represent relation between temperature and Raman peak position. The representative Raman peak are G peak and 2D peak. However, only 2D peak was employed in this experiment, because the shape of 2D peak has much sharper than that of G peak. In this section, the temperature coefficient pertinent to 2D peak was estimated in the temperature range of 300 K – 400 K at every 25 K. The sample was laid on the hot plate (Linkam THMS600), then the temperature was controlled by this hot plate.

4.2.1 Temperature of graphene during the calibration.

In the most experiment that employs the opto-thermal Raman technique assume that the temperature graphene is equal to the temperature of topside of substrate. Additionally, they assume that the temperature of topside of the substrate is equal to the temperature of the hot plate. However, since Bi_2Te_3 has a very low thermal conductivity and a low melting point, the second assumption is not valid. Therefore, the topside of Bi_2Te_3 substrate temperature was measured using K-type thermocouple (Omega). Figure 4.1 indicates the measured temperature of topside of Bi_2Te_3. The black line is the controlled temperature and the red square is the measured temperature. As the controlled temperature is increasing, the difference controlled temperature and topside temperature becomes large due to the increased convection to the air. This measured temperature was

considered as the temperature of graphene when we calibrate the position of Raman 2D peak.

4.2.2 Temperature coefficient of Raman 2D peak

As mentioned before, Raman 2D peak positions were measured in temperature range of 300 K – 400 K per 25 K. The laser power was adjusted to 0.02mW which is enough low to avoid the effect of local heating. Temperature coefficients of Raman 2D peak for 20× objective and 100× objective are shown at Figure 4.2. The Raman 2D peak position of graphene tends to linearly decrease with increasing temperature. This linear dependence on temperature provides temperature coefficients ($d\omega/dT$) for 20× objective and 100× objective were -0.0787 cm^{-1}/K and -0.0785 cm^{-1}/K, respectively. The temperature coefficients are nearly same independent of the magnification of lens. It is not unsurprising that the temperature coefficient does not changes with changing the objectives, because temperature coefficient is not a function of the magnification of the objectives.

4.3 Position of Raman 2D peak depending on laser power

The second procedure for Raman thermometry is a laser heating procedure. In this procedure, 2D peak Raman shift depending on incident laser power ($d\omega/dP$) can be measured. Then, Raman measured temperature can be extracted

from the equation.

$$T_{m\_exp} = \frac{d\omega}{dP} \cdot \frac{dT}{d\omega} \cdot P \tag{4.1}$$

At the heating process, we irradiated the laser power of 0.1 mW and 0.25 mW for 100× objective and 20× objective, respectively. This is relatively low laser power compared to other experiments for the Raman thermometry. Due to the low thermal conductivity and low melting point of Bi_2Te_3, all incident laser power was controlled under 0.5 mW to avoid local sample damage in the paper related to the Raman experiment with Bi_2Te_3. In our experiment, we observed several times of sample damage over 0.3 mW of incident power. However, owing to the high absorptivity of Bi_2Te_3, the sample was heated well despite irradiating the low incident power. In this experiment, the power dependence of Raman shift ($d\omega/dP$) was -11.520 cm^{-1}/mW and -16.7 cm^{-1}/mW for 20× objective and 100× objective, respectively as depicted in Figure 4.3. Using the equation (4.1) and the coefficients obtained from previous two procedures, obtained Raman measured temperature of graphene were 336.59 K and 321.27 K for 100× objective and 20× objective, respectively.

4.4 Result of the opto-thermal Raman technique

The solution curves from numerical calculations and Raman thermometry for

two objectives were represented in Figure 4.4. The solution sets were obtained per every 10 W/m·K for each lens. The slope of the solution curve for 20× objective was steeper than that of the solution curve for 100× objective. Since the thermal properties do not change much in the region of measured temperature and the magnification of objectives, the intersection point could be considered as a final single solution set. In Figure 4.4, extracted thermal contact conductance was 4.160×10^6 W/m^2·K and thermal conductivity of graphene was 438.71 W/m·K.

4.5 Repeatability and accuracy of the method

The repeatability and accuracy of the result value should be validated for our experiment, because the thermal properties between graphene and Bi_2Te_3 has not been reported. For the repeatability, we performed 10 more same experiments at the different locations of our sample. The repeatability of result values is portrayed in Figure 4.5. The results of 11 times of experiment (red shaded ellipse) are $(3.454 \pm 0.416) \times 10^6$ W/m^2·K for the thermal contact conductance and 411.589 ± 54.322 W/m·K for the thermal conductivity. The statistical uncertainty of our experiment is slightly high. This results from the low laser power to avoid damage of Bi_2Te_3 at the heating procedure could contribute this large uncertainty. Usually, more than one values of laser power are used at the heating procedure to obtain dependence power of Raman peak shift ($d\omega/dP$) (Malekpour et al., 2016).

A slope of linear curve can be more accurate when the number of points are increased. However, we just used two point to obtain dependence power of Raman peak shift *(dω/dP*) due to the power limitation. This might increase the uncertainty of our experiment. Furthermore, another possible reason for large uncertainty is the resolution and orthogonality of solution curve. Our result value of k_g and G_c comes from the intersection point of two solution curves. Since both two solution curves can simultaneously move in the region of temperature uncertainty, the intersection point can be formed in this region. Additionally, having different resolution per temperature, two solution curves cannot help make a large uncertainty area.

For the accuracy, we can compare our data to the previous reported results at Table 4.1. In this case, our thermal conductivity would be employed due to the absence of published thermal contact conductance value for the graphene/Bi_2Te_3 interface. The generally known thermal conductivity of supported graphene is 300-700 W/m·K. Fortunately, our measured thermal conductivity of graphene is in this interval. on the other hands, Reported values of thermal contact conductance with other substrate have two~eight orders of value. Although it cannot be compared with our values, it could be criterion that our result is not unrealistic.

4.6 Combination of objectives

We performed the entirely same experiment with 100×, 50× and 20× objectives at the same locations. As shown in Figure 4.6 (above), we observed nearly same value of temperature coefficient regardless of the magnification of lens. The obtained temperature coefficients were -0.0787 cm^{-1}/K, -0.078cm^{-1}/K and -0.785cm^{-1}/K for 20×, 50× and 100× objectives, respectively. However, the slopes of solution curve for each lens were slightly different. The largest orthogonality was observed at the combination of 100× and 20× due to the large difference of magnification. Slightly different solution sets of thermal conductivity (k_g) and thermal contact conductance (G_c) were obtained. The extracted solution sets (k_g, G_c) were (340 W/m·K, 2.969×10^6 $W/m^2\cdot K$) for 50× & 100× objectives, (420.78 W/m·K, 3.897×10^6 $W/m^2\cdot K$) for 20× & 100× objectives, and (510.891 W/m·K, 6.182×10^6 $W/m^2\cdot K$) for 50× & 100× objectives as shown in Figure 4.6 (below). This difference attributed that the resolution of solution curve pertaining temperature is significantly different. However, not so much different was observed among all these result values. In our experiment, the orthogonality was considered as an important factor determining the solution set, because slight change of temperature from Opto-thermal Raman thermometry may have large influence on the result values when the solution curves have a small orthogonality. Therefore, combination 100× and 20× objectives with the largest orthogonality was chosen as our lens combination.

4.7 Limitation of laser power

There is an issue about a limitation of laser power when Bi_2Te_3 is used in Raman spectroscopy. As noticed before, since Bi_2Te_3 has a very low thermal conductivity and a low melting point, Bi_2Te_3 can be easily damaged by the local heating. As shown in Figure 4.7, we observed that sample was damaged after laser above 0.3 mW was irradiated. In the yellow circle in Figure 4.7 (below), 3 points (defect) are generated compared to red circle in Figure 4.7 (above) due to the high laser power. Therefore, all incident laser power were controlled below 0.3 mW to avoid any sample damages.

4.8 Conclusion

In this chapter, results pertaining to the opto-thermal Raman technique were represented. Temperature dependence of 2D peak, Power dependence of 2D peak and extracted graphene thermal conductivity and thermal contact conductance were reported. Furthermore, why 20× and 100× objectives were chosen for our experiment was explained in this chapter.

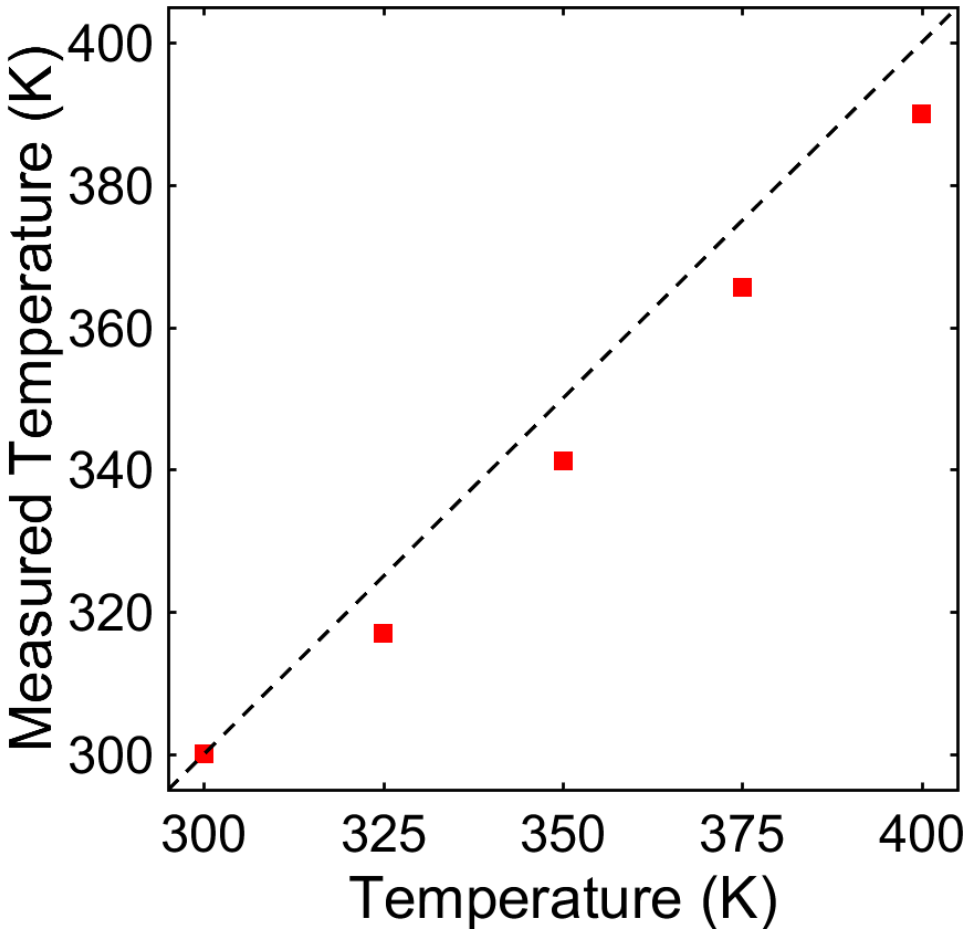

Figure 4.1 Temperature of topside of Bi_2Te_3 substrate on a hot plate measured by K-type thermocouple.

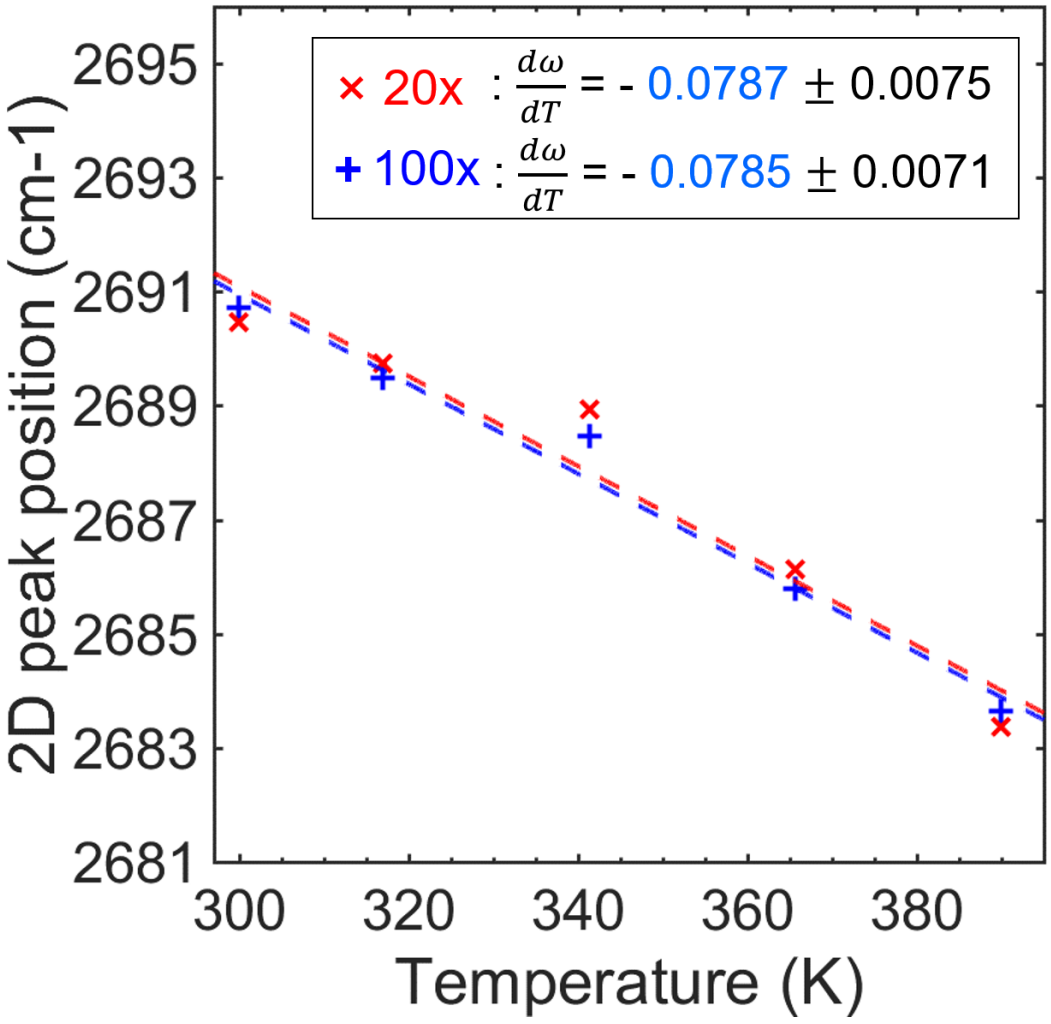

Figure 4.2 The relation between Raman 2D peak and temperature of graphene for 20× (red) and 100× (blue) objectives.

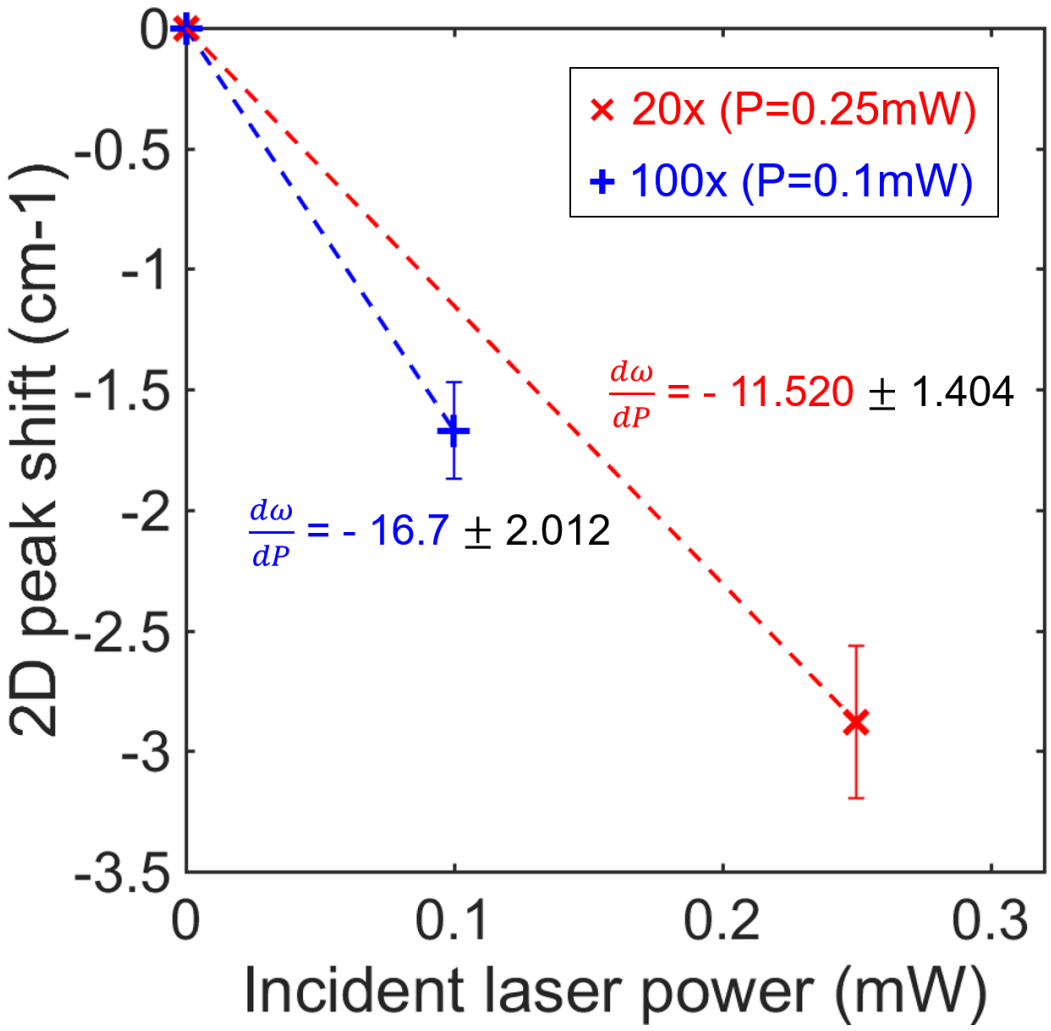

Figure 4.3 The relation between Raman 2D peak and laser power for 20× (red) and 100× (blue) objectives.

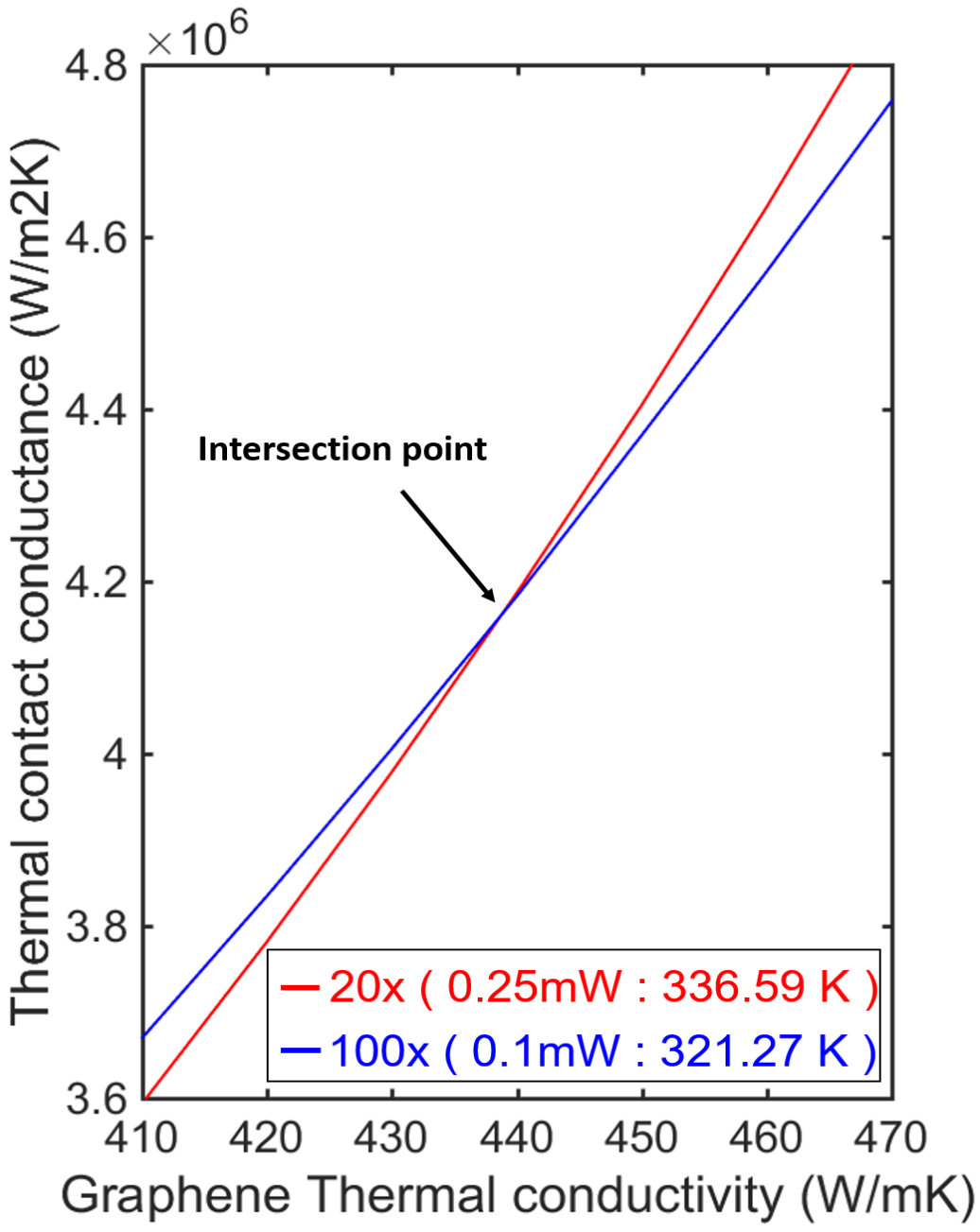

Figure 4.4 Two solution curves of each governing equation for 20× (red) and 100× (blue) objectives and its intersection point.

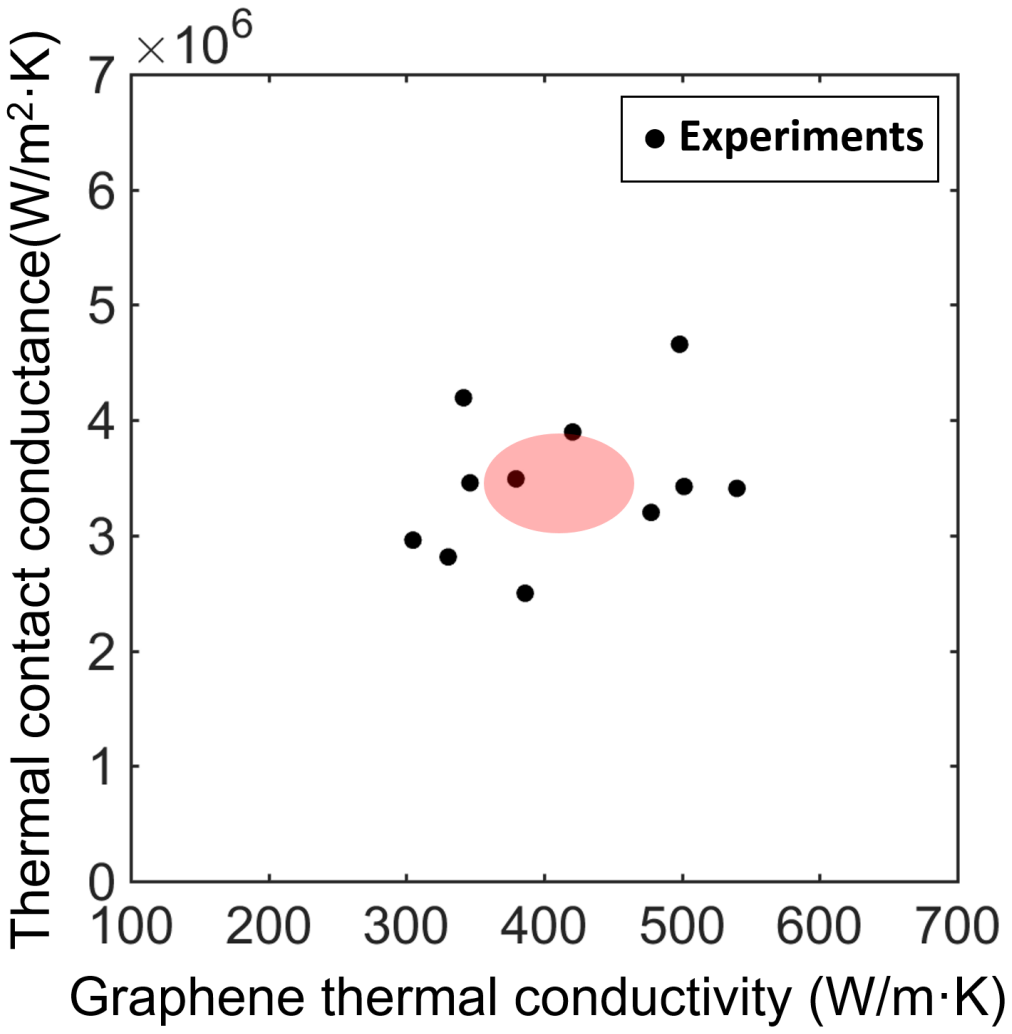

Figure 4.5 Result values of (k_g & G_c) for 11 experiment (Black dots) and its statistical uncertainty (Red ellipse)

Reference	**Descriptions**	**Thermal conductivity (W/m·K.)**	**Thermal contact conductance ($W/m^2 \cdot K.$)**	**Method**
This work	Graphene/Bi_2Te_3	411.589±54.322	(3.454±0.416)×10^6	Opto-thermal Raman thermometry
Kim, *et al*	Graphene/SiO_2	642±138	-	
Judek, *et al*	Graphene/SiO_2	307.9±0.4	(1.62±0.01)×10^6	
Seol, *et al*	Graphene/SiO_2	600	-	Raman spectroscopy
Zhao, *et al*	Graphene/SiO_2	179(+111/-86)	340(+327/-80)	Electrical heating and Raman probing
Yue et al	Graphene/SiC	-	(1.736~2.066)×10^7	
Tang, *et al*	Graphene/SiO_2	-	183±10	Photon heating and Raman probing
Tang, *et al*[2]	Graphene/Si	-	266±10	
Tang, *et al*[6]	Graphene/SiC	-	410±7	
Chen, *et al*	Graphene/SiO_2	-	(8.333~17.857)×10^7	3ω method
Mak *et al*	Graphene/SiO_2	-	(2~11)×10^7	Pump-probe method
Chung et al	Graphene/SiO_2	-	(5.076~6.993)×10^5	Scanning Thermal Microscopy

Table 4.1 Experimental results for thermal conductivity and thermal contact conductance at graphene and its substrate.

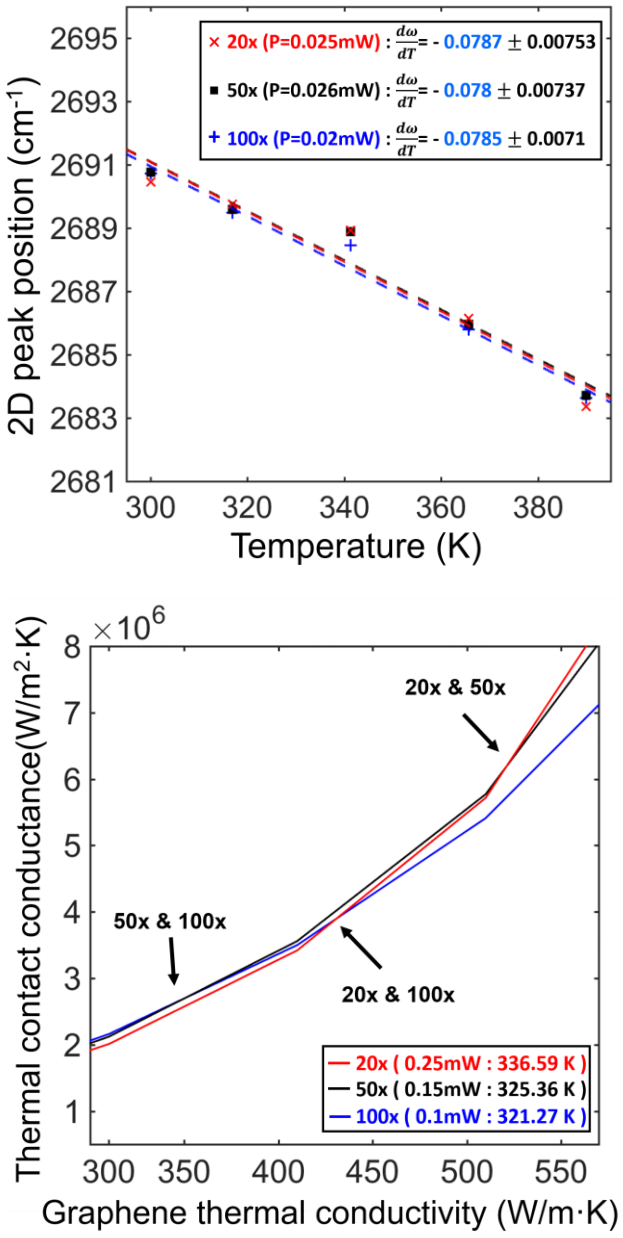

Figure 4.6 Temperature dependence of Raman 2D peak for three objectives and result values using 3 types of objectives.

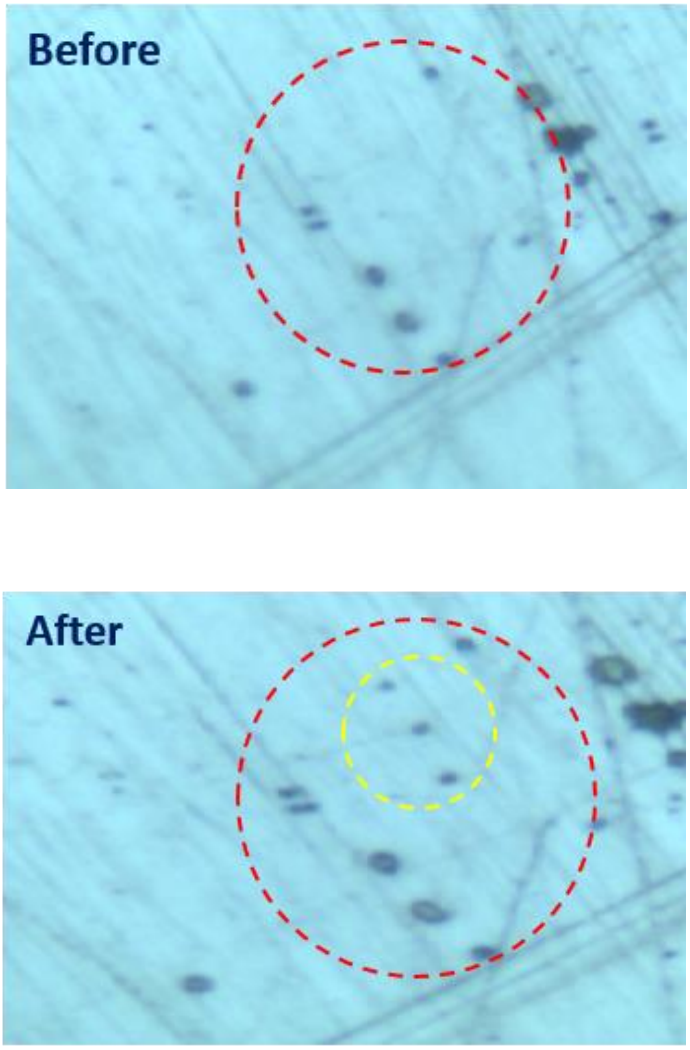

Figure 4.7 Optical image of sample before damage (above), after damage (below) under high laser power.

Chapter 5

Summary and Conclusions

In this study, thermal properties at the interface of graphene and Bi_2Te_3 substrate were measured using an opto-thermal Raman technique with two different objectives.

In Chapter 2, procedure to prepare sample was presented in detail. Single layer graphene with a high quality was synthesized by CVD method with copper foil as a catalyst layer and methane gas as a precursor. Moreover, Bi_2Te_3 substrate was synthesized by Bridgman method, followed by ball-milling procedure, sintering process. Then, synthesized graphene was transferred to the Bi_2Te_3 substrate using PMMA transfer method. After synthesis and transfer, characterizations of samples were proceeded using SEM image, Raman spectroscopy, Raman mapping, optical microscopy. These characterization reveals that synthesized graphene has a large area to perform measurement and graphene on the Bi_2Te_3 substrate was successfully transferred.

In Chapter 3, method for measurement, an opto-thermal Raman technique with two different objectives, was introduced. The opto-thermal Raman technique consists of Raman thermometry to experimentally measure temperature of graphene at the given laser power and numerical calculation to extract thermal

properties to make condition that temperature of graphene from governing equations is equal to temperature of graphene from Raman thermometry. Moreover, how to obtain absorptivity of supported graphene which is one of the main difficulty of the opto-thermal Raman technique was presented in Chapter 3. Complex refractive index and Fresnel's equation was employed to extract the absorptivity of graphene and its substrate.

In Chapter 4, results of the opto-thermal Raman technique were depicted. Temperature of surface of Bi_2Te_3 substrate for Raman calibration, temperature vs Raman peak positions, and laser power vs Raman peak position have been measured. Since we employed two different objectives, two solution curves were obtained from each objectives. The property is not a function of the magnifications of objective, the intersection point can be considered as a single solution set for graphene thermal conductivity and thermal contact conductance. Using these relations and solving governing equations thermal properties were extracted. Furthermore, repeatability and accuracy of improved Raman technique were examined. Total 11 experiments were implemented to verify repeatability of our experiment. Although slightly large uncertainty was obtained, the result values were in the range of known values. Furthermore, result values were compared with those of other substrate, since no experimental data or theoretical prediction has been reported for graphene and Bi_2Te_3. As a result, we can verify our measured values are not unrealistic values since result values have similar orders with other values

In conclusion, thermal properties at the interface of graphene and Bi_2Te_3 were firstly measured using the opto-thermal Raman technique. Moreover, previous opto-thermal Raman technique for supported graphene was improved, since the absorptivity of graphene and its substrate was extracted from Fresnel's equation with complex refractive index of each material. Lastly, Thermal properties extracted in this study can be used as fundamental properties to design the composite of graphene and Bi_2Te_3 and optimize its performance.

References

Teweldebrhan, D., Goyal, V. & Balandin, A. A. 2010, Exfoliation and Characterization of Bismuth Telluride Atomic Quintuples and Quasi-Two-Dimensional Crystals. *Nano Letters*, 10, 1209-1218.

Snyder, G. J. & Toberer, E. S. 2008, Complex Thermoelectric Materials. *Nature Materials*, 7, 105.

Park, H., Kim, D., Eom, Y., Wijethunge, D., Hwang, J., Kim, H. & Kim, W. 2017, Mat-Like Flexible Thermoelectric System Based on Rigid Inorganic Bulk Materials. *Journal of Physics D: Applied Physics*, 50, 494006.

Yim, W. & Rosi, F. 1972, Compound Tellurides and Their Alloys for Peltier Cooling—a Review. *Solid-State Electron*, 15, 1121-1140.

Jeong, S. H., Cruz, F. J., Chen, S., Gravier, L., Liu, J., Wu, Z., Hjort, K., Zhang, S.-L. & Zhang, Z.-B. 2017, Stretchable Thermoelectric Generators Metallized with Liquid Alloy. *ACS Applied Materials & Interfaces*, 9, 15791-15797.

Kim, C. S., Lee, G. S., Choi, H., Kim, Y. J., Yang, H. M., Lim, S. H., Lee, S.-G. &

Cho, B. J. 2018, Structural Design of a Flexible Thermoelectric Power Generator for Wearable Applications. *Applied Energy*, 214, 131-138.

Beyer, H., Nurnus, J., Böttner, H., Lambrecht, A., Wagner, E. & Bauer, G. 2002, High Thermoelectric Figure of Merit Zt in Pbte and Bi_2Te_3-Based Superlattices by a Reduction of the Thermal Conductivity. *Physica E (Amsterdam, Neth.)*, 13, 965-968.

Kim, W., Zide, J., Gossard, A., Klenov, D., Stemmer, S., Shakouri, A. & Majumdar, A. 2006, Thermal Conductivity Reduction and Thermoelectric Figure of Merit Increase by Embedding Nanoparticles in Crystalline Semiconductors. *Physical Review Letters*, 96, 045901.

Venkatasubramanian, R. 2000, Lattice Thermal Conductivity Reduction and Phonon Localizationlike Behavior in Superlattice Structures. *Physical Review B*, 61, 3091.

Geim, A. K. & Novoselov, K. S. 2007, The Rise of Graphene. *Nature Materials*, 6, 183.

Seol, J. H., Jo, I., Moore, A. L., Lindsay, L., Aitken, Z. H., Pettes, M. T., Li, X. Yao, Z., Huang, R. & Broido, D. 2010, Two-Dimensional Phonon Transport in

Supported Graphene. *Science*, 328, 213-216.

Balandin, A. A., Ghosh, S., Bao, W., Calizo, I., Teweldebrhan, D., Miao, F. & Lau, C. N. 2008, Superior Thermal Conductivity of Single-Layer Graphene. *Nano Letters*, 8, 902-907.

Anno, Y., Imakita, Y., Takei, K., Akita, S. & Arie, T. 2017, Enhancement of Graphene Thermoelectric Performance through Defect Engineering. *2D Materials*, 4, 025019.

Wang, C.-R., Lu, W.-S., Hao, L., Lee, W.-L., Lee, T.-K., Lin, F., Cheng, I.-C. & Chen, J.-Z. 2011, Enhanced Thermoelectric Power in Dual-Gated Bilayer Graphene. *Physical Review. Letters*, 107, 186602.

Xiao, N., Dong, X., Song, L., Liu, D., Tay, Y., Wu, S., Li, L.-J., Zhao, Y., Yu, T. & Zhang, H. 2011, Enhanced Thermopower of Graphene Films with Oxygen Plasma Treatment. *ACS Nano*, 5, 2749-2755.

Lee, W., Kihm, K. D., Kim, H. G., Shin, S., Lee, C., Park, J. S., Cheon, S., Kwon, O. M., Lim, G. & Lee, W. 2017, In-Plane Thermal Conductivity of Polycrystalline Chemical Vapor Deposition Graphene with Controlled Grain Sizes. *Nano Letters*, 17, 2361-2366.

Cahill, D. G., Braun, P. V., Chen, G., Clarke, D. R., Fan, S., Goodson, K. E., Keblinski, P., King, W. P., Mahan, G. D. & Majumdar, A. 2014, Nanoscale Thermal Transport. Ii. 2003–2012. *Applied Physics Reviews*, 1, 011305.

Nika, D., Pokatilov, E., Askerov, A. & Balandin, A. 2009, Phonon Thermal Conduction in Graphene: Role of Umklapp and Edge Roughness Scattering. *Physical Review B*, 79, 155413.

Agarwal, K., Kaushik, V., Varandani, D., Dhar, A. & Mehta, B. 2016, Nanoscale Thermoelectric Properties of Bi_2Te_3–Graphene Nanocomposites: Conducting Atomic Force, Scanning Thermal and Kelvin Probe Microscopy Studies. *Journal of Alloys and Compounds*, 681, 394-401.

Ju, H. & Kim, J. 2016, Preparation and Structure Dependent Thermoelectric Properties of Nanostructured Bulk Bismuth Telluride with Graphene. *Journal of. Alloys and Compounds*, 664, 639-647.

Li, A., Shahbazi, M., Zhou, S., Wang, G., Zhang, C., Jood, P., Peleckis, G., Du, Y., Cheng, Z. & Wang, X. 2010, Electronic Structure and Thermoelectric Properties of Bi_2Te_3 Crystals and Graphene-Doped Bi_2Te_3. *Thin Solid Films*, 518, e57-e60.

Liang, B., Song, Z., Wang, M., Wang, L. & Jiang, W. 2013, Fabrication and

Thermoelectric Properties of Graphene/Bi_2Te_3 Composite Materials. *Journal of Nanomaterials*, 6.

Dong, J., Liu, W., Li, H., Su, X., Tang, X. & Uher, C. 2013, In Situ Synthesis and Thermoelectric Properties of PbTe–Graphene Nanocomposites by Utilizing a Facile and Novel Wet Chemical Method. *Journal of Materials Chemistry A*, 1, 12503-12511.

Wang, S., Li, H., Qi, D., Xie, W. & Tang, X. 2011, Enhancement of the Thermoelectric Performance of B-Zn_4Sb_3 by in Situ Nanostructures and Minute Cd-Doping. *Acta Materialia*, 59, 4805-4817.

Xie, W., Tang, X., Yan, Y., Zhang, Q. & Tritt, T. M. 2009, Unique Nanostructures and Enhanced Thermoelectric Performance of Melt-Spun Bisbte Alloys. *Applied Physics Letters*, 94, 102111.

Yue, Y., Zhang, J., Tang, X., Xu, S. & Wang, X. 2015, Thermal Transport across Atomic-Layer Material Interfaces. *Nanotechnology Reviews*, 4, 533-555.

Chen, C.-C., Li, Z., Shi, L. & Cronin, S. B. 2014, Thermal Interface Conductance across a Graphene/Hexagonal Boron Nitride Heterojunction. *Applied Physics Letters*, 104, 081908.

Chen, Z., Jang, W., Bao, W., Lau, C. & Dames, C. 2009, Thermal Contact Resistance between Graphene and Silicon Dioxide. *Applied Physics Letters*, 95, 161910.

Chung, J., Hwang, G., Kim, H., Yang, W. & Kwon, O. 2015, Towards an Accurate Measurement of Thermal Contact Resistance at Chemical Vapor Deposition-Grown Graphene/SiO_2 Interface through Null Point Scanning Thermal Microscopy. *Journal of Nanoscience and Nanotechnology*, 15, 9077-9082.

Hopkins, P. E., Baraket, M., Barnat, E. V., Beechem, T. E., Kearney, S. P., Duda, J. C., Robinson, J. T. & Walton, S. G. 2012, Manipulating Thermal Conductance at Metal–Graphene Contacts Via Chemical Functionalization. *Nano Letters*, 12, 590-595.

Mak, K. F., Lui, C. H. & Heinz, T. F. 2010, Measurement of the Thermal Conductance of the Graphene/SiO_2 Interface. *Applied Physics Letters*, 97, 221904.

Tang, X., Xu, S., Zhang, J. & Wang, X. 2014, Five Orders of Magnitude Reduction in Energy Coupling across Corrugated Graphene/Substrate Interfaces. *ACS Applied Materials & Interfaces*, 6, 2809-2818.

Ferrari, A. C. & Basko, D. M. 2013, Raman Spectroscopy as a Versatile Tool for

Studying the Properties of Graphene. *Nature Natnotechnology*, 8, 235.

Yue, Y., Zhang, J. & Wang, X. 2011, Micro/Nanoscale Spatial Resolution Temperature Probing for the Interfacial Thermal Characterization of Epitaxial Graphene on 4H-SiC. *Small*, 7, 3324-3333.

Liu, Y., Ong, Z.-Y., Wu, J., Zhao, Y., Watanabe, K., Taniguchi, T., Chi, D., Zhang, G., Thong, J. T. & Qiu, C.-W. 2017, Thermal Conductance of the 2D MoS_2/h-BN and Graphene/h-BN Interfaces. *Scientific Reports*, 7, 43886.

Tang, X., Xu, S. & Wang, X. 2014, Corrugated Epitaxial Graphene/SiC Interfaces: Photon Excitation and Probing. *Nanoscale*, 6, 8822-8830.

Judek, J., Gertych, A. P., Świniarski, M., Łapińska, A., Dużyńska, A. & Zdrojek, M. 2015, High Accuracy Determination of the Thermal Properties of Supported 2D Materials. *Scientific Reports*, 5, 12422.

Taube, A., Judek, J., Łapińska, A. & Zdrojek, M. 2015, Temperature-Dependent Thermal Properties of Supported MoS_2 Monolayers. *ACS Applied Materials & Interfaces*, 7, 5061-5065.

Das, A., Pisana, S., Chakraborty, B., Piscanec, S., Saha, S., Waghmare, U.

Novoselov, K., Krishnamurthy, H., Geim, A. & Ferrari, A. 2008, Monitoring Dopants by Raman Scattering in an Electrochemically Top-Gated Graphene Transistor. *Nature Natnotechnology***,** 3, nnano. 2008.67.

Huang, Y., Dong, X., Shi, Y., Li, C. M., Li, L.-J. & Chen, P. 2010, Nanoelectronic Biosensors Based on CVD Grown Graphene. *Nanoscale*, 2, 1485-1488.

Yang, D., Velamakanni, A., Bozoklu, G., Park, S., Stoller, M., Piner, R. D., Stankovich, S., Jung, I., Field, D. A. & Ventrice Jr, C. A. 2009, Chemical Analysis of Graphene Oxide Films after Heat and Chemical Treatments by X-Ray Photoelectron and Micro-Raman Spectroscopy. *Carbon*, 47, 145-152.

Suk, J. W., Kitt, A. Magnuson, C. W., Hao, Y., Ahmed, S., An, J., Swan, A. K., Goldberg, B. B. & Ruoff, R. S. 2011, Transfer of CVD-Grown Monolayer Graphene onto Arbitrary Substrates. *ACS Nano*, 5, 6916-6924.

Ryu, S., Liu, L., Berciaud, S., Yu, Y.-J., Liu, H., Kim, P., Flynn, G. W. & Brus, L. E. 2010, Atmospheric Oxygen Binding and Hole Doping in Deformed Graphene on a SiO_2 Substrate. *Nano Letters*, 10, 4944-4951.

Cai, W., Moore, A. L., Zhu, Y., Li, X., Chen, S., Shi, L. & Ruoff, R. S. 2010, Thermal Transport in Suspended and Supported Monolayer Graphene Grown by

Chemical Vapor Deposition. *Nano Letters*, 10, 1645-1651.

Chen, S., Moore, A. L., Cai, W., Suk, J. W., An, J., Mishra, C., Amos, C., Magnuson, C. W., Kang, J. & Shi, L. 2010, Raman Measurements of Thermal Transport in Suspended Monolayer Graphene of Variable Sizes in Vacuum and Gaseous Environments. *ACS Nano*, 5, 321-328.

Cheon, S., Kihm, K. D., Kim, H., Lim, G., Park, J. S. & Lee, J. S. 2014, How to Reliably Determine the Complex Refractive Index (Ri) of Graphene by Using Two Independent Measurement Constraints. *Scientific Reports*, 4, 6364.

Malekpour, H., Ramnani, P., Srinivasan, S., Balasubramanian, G., Nika, D. L., Mulchandani, A., Lake, R. K. & Balandin, A. A. 2016, Thermal Conductivity of Graphene with Defects Induced by Electron Beam Irradiation. *Nanoscale*, 8, 14608-14616.

Zhao, W., Chen, W., Yue, Y. & Wu, S. 2017, In-Situ Two-Step Raman Thermometry for Thermal Characterization of Monolayer Graphene Interface Material. *Applied Thermal Engineering*, 113, 481-489.

Appendix

MATLAB codes for numerical calculations

Appendix A. 3D cylindrical coordinate heat transfer model for supported graphene and it substrate

---

```
Nk = 1*10^5;   % number of iterations   <<<<<<<<<<<<<<<<<<<<<<<<----
----- user input !!!!!!!!!!!!
% Domain & geometry-----------------------------------------------
% radius
ddr = 10*10^-9;   %   <<<<<<<<<<<<<<<<<<<<<<<---------- user
input !!!!!!!!!!!!
drmax = 1.0*10^-6;   %   <<<<<<<<<<<<<<<<<<<<<<<<---------- user
input !!!!!!!!!!!!
M = 64;   %   <<<<<<<<<<<<<<<<<<<<<<<<---------- user
input !!!!!!!!!!!!
dr(1) = ddr;
r(1) = 0.5*dr(1);
for i = 2:M
    if dr(i-1) < drmax
        dr(i) = ddr*i;
    else
        dr(i) = drmax;
    end
    r(i) = r(i-1)+dr(i);
end
```

```
dr(M+1) = dr(M);

% Thickness
tg = 0.334*10^-9;

ddz = 0.01*10^-6;   %   <<<<<<<<<<<<<<<<<<<<<<<<---------- user
input !!!!!!!!!!!!
dzmax = 1.0*10^-6;   %   <<<<<<<<<<<<<<<<<<<<<<<<---------- user
input !!!!!!!!!!!!
N = 68 + 2;   %   <<<<<<<<<<<<<<<<<<<<<<<<---------- user
input !!!!!!!!!!!!
tdz(1) = ddz;
for i = 2:N-2
    if tdz(i-1) < dzmax
        tdz(i) = ddz*i;
    else
        tdz(i) = dzmax;
    end
end
for i = 1:N-2
    dz(i) = tdz(N-i-1);
end
z(1) = 0.0;
for i = 2:N-1
    z(i) = z(i-1) + dz(i-1);
end
z(N) = z(N-1);

% Physical properties   <<<<<<<<<<<<<<<<<<<<<<<<---------- user
input !!!!!!!!!!!!
kg = 337.2;  % [W*m^-1*K^-1] graphene   300 ~ 1000
```

```
ko_in = 1.582;   % [W*m^-1*K^-1] Thermal conductivity of Bi2Te3
in_plane direction
ko_cross = 1.057; % [W*m^-1*K^-1] Thermal conductivity of Bi2Te3
cross_plane direction
hB = 0*10^4;   % [W*m^-2*K^-1] bottom-side natural convection heat
transfer coefficient
hT = 2.9*10^4;   % [W*m^-2*K^-1] top-side natural convection heat
transfer coefficient
TBC = 2.941*10^6;   % [W*m^-2*K^-1] 25~178*10^6 W*m^-2*K^-1
thermal boundary conductance between graphene and Bi2Te378



% Laser beam intensity
Q_laser = 0.25*10^-3;   % [W] laser power
<<<<<<<<<<<<<<<<<<<<<<<<--------- user input !!!!!!!!!!!!
absorption_graphene = 0.0084;
absorption_substrate = 0.4411;
lambda = 514*10^-9;   % [m] laser wavelength
NA = 0.4;
r0 = lambda/(pi*NA);   % [m]
q0 = 2*Q_laser*absorption_graphene/(pi*r0^2);   % [W/m^2] maximum
laser power intensity
q0_sub = 2*Q_laser*absorption_substrate/(pi*r0^2);
Q_total = 0.0;
Q_total_graphene = 0.0;
Q_total_sub = 0.0;



for i = 1:M
```

```
    r1 = r(i)-0.5*dr(i);
    r2 = r(i)+0.5*dr(i+1);
    rr1 = r1/r0;
    rr2 = r2/r0;
    q(i) = q0*(r0^2)*0.5*[exp(-2*rr1^2) - exp(-2*rr2^2)]/(r2^2 -
r1^2);   % average laser heat generation per area for i-th control
volume
    Q_total_graphene = Q_total_graphene+q(i)*pi*(r2^2 - r1^2);
end
Q_total_graphene = Q_total_graphene;

for i = 1:M
    r1 = r(i)-0.5*dr(i);
    r2 = r(i)+0.5*dr(i+1);
    rr1 = r1/r0;
    rr2 = r2/r0;
    q_sub(i) = q0_sub*(r0^2)*0.5*[exp(-2*rr1^2) - exp(-
2*rr2^2)]/(r2^2 - r1^2);   % average laser heat generation per
area for i-1th control volume
    Q_total_sub = Q_total_sub+q_sub(i)*pi*(r2^2 - r1^2);
end
Q_total_sub = Q_total_sub;
Q_total = Q_total_graphene + Q_total_sub;



% Temperature; room temperature
T_room = 26.84 + 273.16;   % [K]
% Temperature; Initial condition
for i = 1:M
    for j = 1:N
```

```
        T(i,j) = T_room;
    end
end

%-----------------------------------------------------------------------
% Energy balance; Gauss-Seidel
%-----------------------------------------------------------------------

omega = 1.0;
Tmax = T_room;
% Constants
ktg = kg*tg;

% Coefficients----------------------------------------------------------
r1 = r(1) - 0.5*dr(1);
r2 = r(1) + 0.5*dr(2);
rr = r(1);

B(1,N) = 0;
C(1,N) = r2*ktg/dr(2);
D(1,N) = rr*(r2-r1)*TBC;
E(1,N) = 0;
F(1,N) = rr*(r2-r1)*hT;

A(1,N) = 1/( B(1,N) + C(1,N) + D(1,N) + E(1,N) + F(1,N) );
G(1,N) = rr*(r2-r1)*q(1);

for i = 2:M  % graphene (top)
    r1 = r(i) - 0.5*dr(i);
    r2 = r(i) + 0.5*dr(i+1);
    rr = r(i);
```

```
    B(i,N) = r1*ktg/dr(i);
    C(i,N) = r2*ktg/dr(i+1);
    D(i,N) = rr*(r2-r1)*TBC;
    E(i,N) = 0;
    F(i,N) = rr*(r2-r1)*hT;

    A(i,N) = 1/( B(i,N) + C(i,N) + D(i,N) + E(i,N) + F(i,N) );
    G(i,N) = rr*(r2-r1)*q(i);
end

r1 = r(1) - 0.5*dr(1);
r2 = r(1) + 0.5*dr(2);
rr = r(1);

B(1,N-1) = 0;
C(1,N-1) = r2*(0.5*dz(N-2))*ko_in/dr(2);
D(1,N-1) = rr*(r2-r1)*ko_cross/dz(N-2);
E(1,N-1) = rr*(r2-r1)*TBC;
F(1,N-1) = 0;

A(1,N-1) = 1/( B(1,N-1) + C(1,N-1) + D(1,N-1) + E(1,N-1) + F(1,N-
1) );
G(1,N-1) = rr*(r2-r1)*q_sub(1);

for i = 2:M
    r1 = r(i) - 0.5*dr(i);
    r2 = r(i) + 0.5*dr(i+1);
    rr = r(i);

    B(i,N-1) = r1*(0.5*dz(N-2))*ko_in/dr(i);
```

```
    C(i,N-1) = r2*(0.5*dz(N-2))*ko_in/dr(i+1);
    D(i,N-1) = rr*(r2-r1)*ko_cross/dz(N-2);
    E(i,N-1) = rr*(r2-r1)*TBC;
    F(i,N-1) = 0;

    A(i,N-1) = 1/( B(i,N-1) + C(i,N-1) + D(i,N-1) + E(i,N-1) +
F(i,N-1) );
    G(i,N-1) = rr*(r2-r1)*q_sub(i);
end

for j = 2:N-2
    r1 = r(1) - 0.5*dr(1);
    r2 = r(1) + 0.5*dr(2);
    rr = r(1);

    B(1,j) = 0;
    C(1,j) = r2*0.5*(dz(j-1) + dz(j))*ko_in/dr(2);
    D(1,j) = rr*(r2-r1)*ko_cross/dz(j-1);
    E(1,j) = rr*(r2-r1)*ko_cross/dz(j);
    F(1,j) = 0;

    A(1,j) = 1/( B(1,j) + C(1,j) + D(1,j) + E(1,j) + F(1,j) );
    G(1,j) = 0;

    for i = 2:M
        r1 = r(i) - 0.5*dr(i);
        r2 = r(i) + 0.5*dr(i+1);
        rr = r(i);

        B(i,j) = r1*0.5*(dz(j-1) + dz(j))*ko_in/dr(i);
        C(i,j) = r2*0.5*(dz(j-1) + dz(j))*ko_in/dr(i+1);
```

```
        D(i,j) = rr*(r2-r1)*ko_cross/dz(j-1);
        E(i,j) = rr*(r2-r1)*ko_cross/dz(j);
        F(i,j) = 0;

        A(i,j) = 1/( B(i,j) + C(i,j) + D(i,j) + E(i,j) + F(i,j) );
        G(i,j) = 0;
    end
end

r1 = r(1) - 0.5*dr(1);
r2 = r(1) + 0.5*dr(2);
rr = r(1);

B(1,1) = 0;
C(1,1) = r2*(0.5*dz(1))*ko_in/dr(2);
D(1,1) = 0;
E(1,1) = rr*(r2-r1)*ko_cross/dz(1);
F(1,1) = rr*(r2-r1)*hB;

A(1,1) = 1/( B(1,1) + C(1,1) + D(1,1) + E(1,1) + F(1,1) );
G(1,1) = 0;

for i = 1:M
    r1 = r(i) - 0.5*dr(i);
    r2 = r(i) + 0.5*dr(i+1);
    rr = r(i);

    B(i,1) = r1*(0.5*dz(1))*ko_in/dr(i);
    C(i,1) = r2*(0.5*dz(1))*ko_in/dr(i+1);
    D(i,1) = 0;
    E(i,1) = rr*(r2-r1)*ko_cross/dz(1);
```

```
    F(i,1) = rr*(r2-r1)*hB;

    A(i,1) = 1/( B(i,1) + C(i,1) + D(i,1) + E(i,1) + F(i,1) );
    G(i,1) = 0;
end


% Iteration-----------------------------------------------------------
for k = 1:Nk
    T_pre = T;

    T(1,N) = A(1,N)*[ C(1,N)*T(2,N) + D(1,N)*T(1,N-1) +
F(1,N)*T_room + G(1,N)];
    for i = 2:M-1
        T(i,N) = A(i,N)*[ B(i,N)*T(i-1,N) + C(i,N)*T(i+1,N) +
D(i,N)*T(i,N-1) + F(i,N)*T_room + G(i,N) ];
    end

    T(1,N-1) = A(1,N-1)*[ C(1,N-1)*T(2,N-1) + D(1,N-1)*T(1,N-2) +
E(1,N-1)*T(1,N) + G(1,N-1) ];
    for i = 2:M-1
        T(i,N-1) = A(i,N-1)*[ B(i,N-1)*T(i-1,N-1) + C(i,N-
1)*T(i+1,N-1) + D(i,N-1)*T(i,N-2) + E(i,N-1)*T(i,N) + G(i,N-1) ];
    end

    for j = 2:N-2
        T(1,j) = A(1,j)*[ C(1,j)*T(2,j) + D(1,j)*T(1,j-1) +
E(1,j)*T(1,j+1) + G(1,j) ];
        for i = 2:M-1
            T(i,j) = A(i,j)*[ B(i,j)*T(i-1,j) + C(i,j)*T(i+1,j) +
D(i,j)*T(i,j-1) + E(i,j)*T(i,j+1) + G(i,j) ];
```

```
        end
    end

    T(1,1) = T_room ;
    for i = 2 : M-1
        T(i,1) = T_room ;
    end

    T = T_pre + omega*(T-T_pre);
    eps(k) = abs((T(1,N)-Tmax)/Tmax);
    Tmax = T(1,N);
    Tcenter(k) = Tmax;
end

%-----------------------------------------------------------------
% Assessment of measured temperature Tm
%-----------------------------------------------------------------
Tm = 0;
Tsub = 0;
Tsubb = 0;
denominator = 0;
for i = 1:M
    rr = r(i);
    r1 = rr - 0.5*dr(i);
    r2 = rr + 0.5*dr(i+1);
    rr1 = r1/r0;
    rr2 = r2/r0;
    Tm = Tm + T(i,N)*(r0^2/4)*(exp(-2*(rr1^2)) - exp(-2*(rr2^2)));
    Tsub = Tsub + T(i,N-1)*(r0^2/4)*(exp(-2*(rr1^2)) - exp(-
2*(rr2^2)));
    Tsubb = Tsubb + T(i,N-2)*(r0^2/4)*(exp(-2*(rr1^2)) - exp(-
```

```
2*(rr2^2)));
    denominator = denominator + (r0^2/4)*(exp(-2*(rr1^2)) - exp(-
2*(rr2^2)));
end
Tm = Tm/denominator;
Tsub = Tsub/denominator;
Tsubb = Tsubb/denominator;

%-----------------------------------------------------------------
% Plot
%-----------------------------------------------------------------
for i = 1:k-1
    rNk(i) = i;
end
Q_conv = 0.0;
for i = 1:M
    r1 = r(i)-0.5*dr(i);
    r2 = r(i)+0.5*dr(i+1);
    Q_conv = Q_conv + (hT*(T(i,N)-T_room) + hB*(T(i,1)-
T_room))*pi*(r2^2 - r1^2);
end
subplot(1,3,1)
semilogx(r,T(:,N-1),'r', r,T(:,N),'b',r,T(:,1),'g')
subplot(1,3,2)
loglog(rNk,real(eps(1:k-1)))
subplot(1,3,3)
semilogx(rNk,real(Tcenter(1:k-1)))

Convection_contribution = Q_conv/(Q_total);
R_domain = r(M);
Z_domain = z(N);
```

```
T_top = T(1,N);
T_mid = T(1,round(N/2));
T_bottom = T(1,1);
TBC
Tm
Tsub
```

그래핀과 Bi_2Te_3기판 계면에서의 열물성 측정

서울대학교 대학원
기계항공공학부
편 경 록

요 약

그래핀은 2004년에 발견된 이래로 탁월한 열, 전기, 기계적 특성으로 각광받는 신소재 중 하나이다. 현재, 그래핀 자체로는 낮은 열전 효율로 인하여 열전 분야에서는 크게 주목받지 못하였으나, 치환 도핑, 복합체 등을 통한 열전 효율 향상의 가능성 때문에 열전 소재로서의 그래핀에 대한 관심이 증가하고 있다. 또한, 비스무스 테룰라이드 (Bi_2Te_3)는 열전 분야에서 사용되는 대표적인 물질이다. Bi_2Te_3는 상온에서의 상당히 열전 효율을 갖는 물질로써, 펠티어 소자와 같은 곳에 사용되어 이미 상용화가 진행되고 있는 물질이다.

최근, Bi_2Te_3에 그래핀을 첨가시켜 열전 효율을 향상시키는데 성공한 사례로부터 알 수 있듯이, 그래핀과 Bi_2Te_3의 복합체는 열전소재로서의 가능성을 보이고 있다. 그러나 그래핀과 Bi_2Te_3의 복합체에서 향상된 이유는 Bi_2Te_3에 삽입된 그래핀이 추가적인 포논 산란을 발생시켜 복합체에서의 열전도도를 감소시키는 데 기인하는 것으로 추정된다. 다만, 복합체에서의 종합적인 열전도도가 감소한다는 것은 실험적으로만 관측되었을 뿐, 그 구체적인 원리 및 방법에 대한

물리적 이해는 뒷받침되어 있지 않은 상황이다. 복합체 내에서의 열전달을 이해하기 위해서는 계면에서의 열물성을 측정하는 것이 중요하다.

따라서 본 연구에서는 기존의 광열 라만 방법을 한 단계 발전시켜 그래핀의 열전도도와 그래핀과 Bi_2Te_3 사이의 접촉열전도를 최초로 측정하였다. 지지된 그래핀에서의 광열 라만 방법에서의 가장 큰 문제점은 기판과 그래핀의 흡광율을 직접적으로 측정할 수 있는 방법이 없다는 것이다. 대부분의 연구에서는 매달린 그래핀의 흡광율을 그대로 사용하고 있으나, 기판이 반도체 또는 도체의 경우에는 그래핀과의 전기장의 변화로 인하여 흡광율이 달라질 수 있다. 이러한 문제점으로 인하여 흡광율을 아는 것은 지지된 그래핀의 물성 측정에 있어서 중요하다. 따라서, 본 연구에서는 이러한 문제를 그래핀과 기판의 복소굴절률과 Fresnel 방정식을 통하여 흡광율을 계산함으로써 해결하였고, 계산된 값을 광열 라만 기법에 적용하였다.

따라서, 본 연구에서는 열전도도 감소에 결정적인 역할을 하는 것으로 추정되는 열물성인 그래핀의 열전도도와 그래핀과 Bi_2Te_3 사이의 접촉열전도를 광열 라만 방법을 이용하여 정량적으로 측정함으로써 그래핀과 Bi_2Te_3의 복합체를 합성하고 그 효율을 최적화하는데 필요한 기초적인 물성을 제시할 수 있을 것으로 기대한다.

주요어 : 그래핀, 비스무스 테룰라이드, 열전도도, 접촉열저항, 광열라만기법, 유한차분기법
학번 : 2016-24783